Technical Report # 5-32688
Contract Number NAS8-36955
Delivery Order No. 122

Turbulence Modelling of Flow Fields in Thrust Chambers (5-32688)

Final Technical Report for the Period
June 10, 1991 through September 13, 1992

February 1993

Prepared by:

C. P. Chen *
Y. M. Kim
H. M. Shang
* Authors listed alphabetically

Prepared for:

NASA Marshall Space Flight Center
Attn: Klause Gross
Propulsion Laboratory
Marshall Space Flight Center, AL 32512

NASA
National Aeronautical and Space Agency

Report Document Page

1. Report No. Final Technical	2. Government Accession No.	3. Recipient's Catalog No.
4. Titile and Subtitle Turbulence Modelling of Flow Fields in Thrust Chambers		5. Report Due September 1992 6. Performing Organization Code Research Institute, UAH
7. Author(s) C. P. Chen , * Y. M. Kim, and H. M. Shang * Authors listed alphabetically		8. Performing Organization Report No. 10. Work Unit No. 5-32688
9. Performing Organization Name and Address UAH Research Institute RI E-47 Huntsville, AL 35899		11. Contract or Grant No. NAS8-36955, D.O. 122
12. Sponsoring Agency Name and Address National Aeronautics and Space Administration Washington, D.C. 20546-001 Marshall Space Flight Center, AL 35812		13. Type of report and Period covered Final Technical Report June 10, 1992 - Sept. 13, 1992 14. Sponsoring Agency Code
15. Supplementary Notes		

16.Abstract

Following the consensus of a workshop in Turbulence Modelling for Liquid Rocket Thrust Chambers, the current effort was undertaken to study the effects of second-order closure on the predictions of thermochemical flow fields. To reduce the instability and computational intensity of the full second-order Reynolds Stress Model, an Algebraic Stress Model (ASM) coupled with a two-layer near wall treatment was developed. Various test problems, including the compressible boundary layer with adiabatic and cooled walls, recirculating flows, swirling flows and the entire SSME nozzle flow were studied to assess the performance of the current model. Detailed calculations for the SSME exit wall flow around the nozzle manifold were executed. As to the overall flow predictions, the ASM removes another assumption for appropriate comparison with experimental data to account for the non-isotropic turbulence effects.

17. Key Words (Suggested by Author(s)) Turbulence, Combustion, Swirling Flows, Non-Isotropic Effects, Compressible Effects		18. Distribution Statement TBD	
19. Security Class. (of this report) Unclassified	20. Security Class. (of this page) Unclassified	21. No. of pages 24 + Appendices	22. Price

NASA FORM 1626 OCT 86

TABLE OF CONTENTS

ABSTRACT

Following the consensus of a workshop in Turbulence Modeling for Liquid Rocket Thrust Chambers, the current effort was undertaken to study the effects of second-order closure on the predictions of thermochemical flow fields. To reduce the instability and computational intensity of the full second-order Reynolds Stress Model, an Algebraic Stress Model (ASM) coupled with a two-layer near wall treatment was developed. Various test problems, including the compressible boundary layer with adiabatic and cooled walls, recirculating flows, swirling flows and the entire SSME nozzle flow were studied to assess the performance of the current model. Detailed calculations for the SSME exit wall flow around the nozzle manifold were executed. As to the overall flow predictions, the ASM removes another assumption for appropriate comparison with experimental data, to account for the non-isotropic turbulence effects.

Acknowlegement

This research is sponsered by NASA-Marshall Space Flight Center under NAS8-36955, D.O. 122. The authors wish to acknowledge the technical guidance of Mr. Klaus Gross of MSFC. The CRAY CPU time supplied by the Alabama Supercomputer Network through UAH is also acknowledged.

1. INTRODUCTION

Thermochemical flow fields of liquid rocket thrust chambers are highly irregular in nature. The momentum fluxes as well as the scalar fluxes, due to the random velocity fluctuations, are usually much greater than the molecular (or laminar) fluxes. Proper descriptions of the turbulent mixing is the key of understanding and predicting reacting flow fields in thrust chambers.

One of the most important features of the flow field analysis in the thrust chamber is to describe the turbulence structure, which correctly includes the variable density effects. In combusting flows, they are caused mainly by chemical reaction, mixture of gases with different densities, including multi-phase interactions, and strong distortion caused by shock boundary layer interactions. Complexity due to compressible combusting turbulence concerning the fluctuating density, leads to more non-linear equations to be solved and to more intractable modeling problems.

Currently, methods of simulating turbulent flows can be classified in the following way: 1) Empirical Correlations, 2) Integral Methods, 3) One-point Closure Methods, 4) Two-point Closure Methods, 5) Large eddy simulation (L.E.S) and 6) Direct numerical simulation (D.N.S). Moving downwards in the list, each method requires more computational resources and fewer modeling assumptions. However, the higher level simulations also require more complex input data to calibrate the models. Such information is very difficult to obtain and often not as accurately known. Therefore, a simulation at a given level is not always more accurate than simulations at lower levels, which applies especially to level 2, 3 and perhaps 4. Due to the tremendous cost of simulating even the simple flows with high level L.E.S and full direct simulations on present day computers, and considering also the trade-off between accuracy and computation time, the one-point closure methods seem to offer the best compromise for engineering technology applications at the present time. The one-point closure methodology includes: (i) Gradient Transport Models and (ii) Reynolds Stress Models. In (i) the construction of an eddy viscosity can be further classified into : (a) equilibrium models, which are essentially mixing length type models; and (b) non-equilibrium models, which include one and two equation models, Reynolds Stress and Algebraic Stress models.

Combustion can affect turbulent transport through the production of density variations,buoyancy, dilatation due to heat release, influence on molecular transport, instabilities and so on. These effects are not well understood now. By and large, empirical closures and model equations are carried over from the Reynolds-averaging procedure for constant density non-reacting flows to the density-weighted (or Favre-averaged) form for turbulent reacting flows. In doing so, physical interpretations of the individual terms can be clearer than for the case with unweighted averaging. However, extra density fluctuating coupled terms, appearing in the transport equations, require extensive modeling efforts. New experimental data is needed to validate the modeling of these new terms.

The main purpose of this proposed study is to incorporate a model which contains sufficient flow physics, encountered in the thrust chamber, and yet is computationally effective to include chemistry/droplet/multiphase effects into a CFD code, to systematically evaluate/assess the performance of the model. In the following, the proposed methodology and proposed tasks will be described.

2. PHYSICAL MODELS

In compressible flows, the statistical description of turbulent flow fields is derived by expressing the dependent variables as the sum of mean and fluctuating quantities and then ensemble-averaging the instantaneous transport equations. Due to the variations and fluctuations of the fluid density, which are more likely to occur in reacting flows with large temperature differences, it is advantageous [1,2,3] to use mass-weighted (or density-weighted) averaging procedures for describing the mean flow features. In chemically reacting flows the instantaneous velocities and temperatures of the fluid are averaged with density-weighting, and density and pressure are merely ensemble-averaged without weighting. Thus, for example,

$$u_i = \tilde{u}_i + u_i'' \tag{1}$$

$$\rho = \bar{\rho} + \rho' \tag{2}$$

and

$$\tilde{u}_i = \overline{\rho u_i} / \bar{\rho} \tag{3}$$

also

$$\overline{\rho u_i''} = 0 \tag{4}$$

$$\overline{u_i''} = -\overline{\rho' u_i''} / \bar{\rho} \neq 0 \tag{5}$$

Equation (5) is important, because most models of compressible turbulent flows in current use neglect such terms or their divergence, which may introduce problems in chemical reacting flows.

The resulting statistical equations for the mass, momentum, energy fields as well as species in turbulent flows are

$$\frac{\partial \bar{\rho}}{\partial t} + \frac{\partial}{\partial x_i}(\bar{\rho}\tilde{u}_i) = 0 \tag{6}$$

$$\frac{\partial \bar{\rho}\tilde{u}_i}{\partial t} + \frac{\partial}{\partial x_j}(\bar{\rho}\tilde{u}_i\tilde{u}_j) = -\frac{\partial}{\partial x_i}\bar{P} + \frac{\partial}{\partial x_j}(\mu\tilde{S}_{ij}) - \frac{\partial}{\partial x_j}(\overline{\rho u_i'' u_j''}) \tag{7}$$

$$\frac{\partial}{\partial t}(\bar{\rho}\tilde{h}) + \frac{\partial}{\partial x_j}(\bar{\rho}\tilde{u}_j\tilde{h}) = \frac{\partial \bar{P}}{\partial t} + \frac{\partial}{\partial x_j}\left(\frac{\mu}{P_r}\frac{\partial \tilde{h}}{\partial x_j} + \frac{\mu}{P_r}\frac{\partial \tilde{h}''}{\partial x_j} - \overline{\rho h'' u_j''}\right) + \tilde{u}_j\frac{\partial \bar{P}}{\partial x_j} + \overline{u_j''\frac{\partial P}{\partial x_j}} + \frac{\partial \bar{Q}}{\partial t} + \bar{\Phi} \quad (8)$$

$$\frac{\partial}{\partial t}(\bar{\rho}\tilde{Y}_k) + \frac{\partial}{\partial x_i}(\bar{\rho}\tilde{Y}_k\tilde{u}_i) = \frac{\partial}{\partial x_i}\left(D\bar{\rho}\frac{\partial \tilde{Y}_k}{\partial x_i} - \overline{\rho Y_k'' u_i''}\right) + \frac{\partial}{\partial x_i}\overline{D\rho\frac{\partial Y_k''}{\partial x_i}} + \overline{\dot{\omega}_k} \quad (9)$$

where the mean strain is

$$S_{ij} = \frac{\partial u_i}{\partial x_j} + \frac{\partial u_j}{\partial x_i} - \frac{2}{3}\delta_{ij}\frac{\partial u_k}{\partial x_k}$$

and

$$\bar{\Phi} = \overline{S_{ij}\frac{\partial u_i}{\partial x_j}}$$

Note that the density-weighted averaging produces forms in the mean momentum equations which are similar term by term to their incompressible counterparts. As mentioned in the introduction section of this report, the main task of the current one-point statistical turbulence modeling is to evaluate the Reynolds stresses, which appear as the last term in equation (7), as well as second order terms in the energy and species equations.

1). Eddy Viscosity Models

At the simplest level of modeling, an explicit algebraic constitutive relationship between the Reynolds stress and the mean strain rate of the flow has been postulated. This requirement utilizes the concept of an eddy viscosity as a ratio of proportionality. From a numerical point of view, this relationship is very convenient, since the eddy viscosity can be combined with the fluid kinematic viscosity to form an "effective " viscosity. It thus allows simple modification of a CFD code, originally developed for laminar flows, to account for turbulence.

The simplest constitutive relationship for expressing Reynolds stress is the classic Boussinesq form, which is still the most popular one:

$$-\overline{\rho u_i'' u_j''} = \mu_t\left(\frac{\partial \tilde{u}_i}{\partial x_j} + \frac{\partial \tilde{u}_j}{\partial x_i} - \frac{2}{3}\delta_{ij}\frac{\partial \tilde{u}_l}{\partial x_l}\right) - \frac{2}{3}\delta_{ij}\bar{\rho}k \tag{10}$$

At this level of the model, the major concern is the estimation of the eddy viscosity μ_t. In general, the eddy viscosity is expressed in terms of a characteristic turbulence velocity scale u', a characteristic length scale l', and an empirically determined constant c_μ. Turbulence models, based on the Boussinesq expression, include zero-equation (mixing length) models [5,6,7], two-equation (with or without modifications of variable density effects) [8-13], and multiple-scale models associated with eddy viscosity estimations. This level of modeling is still the most widely used model in most engineering calculations. However, the major drawback of the Boussinesq expression is that the constitutive assumption implies an isotropic turbulence field. Past results show that for many complex flows, especially for shear driven flows such as the ones experienced in the coaxial injector jet flows in the combustor of a thrust chamber, this type of modeling usually fails to predict the turbulent flow field correctly.

2). <u>Second Order Models</u>

Recently, a workshop was held [16] in which the currently used turbulence models were reviewed. Based on the consensus of the workshop, models based on second-order closures were recommended. During the following activity, addressing the second order modeling level, the constitutive assumption such as eq.(10) was totally abandoned and a transport equation for the Reynolds stress was derived. By manipulating the instantaneous Navier-Stokes equation, the field equations representing Reynolds stress can be obtained:

$$\frac{D}{Dt}\overline{\rho u_i'' u_j''} = P_{ij} + D_{ij} + \pi_{ij} + C_{ij} - \varepsilon_{ij} \tag{11}$$

To date, equation (11) still represents the most complex turbulence model, used in computational fluid dynamic problems, in which anisotropy and extra complex strains can be automatically accounted for. The symbols and their physical mechanism as well as their mathematical forms are given in Table 1. These terms contain a multitude of new turbulence moments involving pressure fluctuation, velocity fluctuations, velocity gradients, and third order correlations. Except for the production terms, the other terms require appropriate modeling to close the set of equations. Detailed experimental data are required to guide these modelings. However, at this stage, there are no reliable data available especially for reacting shear layers to give any guidance on the model development. Consequently, the validity of several terms in the model can only be inferred indirectly from the behavior of the mean motions and some budget profiles across some simpler flows. For three-dimensional flow calculations, six Reynolds-stress equations have to be solved which introduce a severe computer cost penalty. To alleviate this problem, but retain the advantages of this level of modeling, a simplified version is recommended.

The Algebraic Stress model proposed by Rodi[4] is based on the assumption that the difference of advection (convection + diffusion) of Reynolds stress and its diffusion transport is proportional to the corresponding difference in turbulent kinetic energy, which implies

$$\frac{D}{Dt}\overline{\rho u_i'' u_j''} - D_{ij} = \frac{\overline{\rho u_i'' u_j''}}{k}\left(\frac{Dk}{Dt} - D_k\right)$$

Thus

$$\overline{\rho u_i'' u_j''} = \frac{k(P_{ij} + \pi_{ij} - \varepsilon_{ij} + C_{ij})}{P_k + C_k - \varepsilon} \tag{12}$$

Terms in Reynolds Stress Equation

$$P_{ij} = \text{Production Tensor} = -\overline{\rho}[\widetilde{u_i''u_k''}\frac{\partial \tilde{u}_j}{\partial x_k} + \widetilde{u_j''u_k''}\frac{\partial \tilde{u}_i}{\partial x_k}]$$

$$D_{ij} = \text{Diffusion Tensor}$$

$$= -\frac{\partial}{\partial x_k}[\overline{\rho}\widetilde{u_i''u_j''u_k''} + \delta_{ik}\overline{u_j''p'} + \delta_{jk}\overline{u_i''p'} - (\mu\overline{S_{ik}u_j''} + \mu\overline{S_{jk}u_i''})]$$

$$\Pi_{ij} = \text{Energy Transfer Tensor} = \overline{p'(\frac{\partial u_i''}{\partial x_j} + \frac{\partial u_j''}{\partial x_i})}$$

$$C_{ij} = \text{Compressibility Tensor} = -[\widetilde{u_i''}\frac{\partial \overline{p}}{\partial x_j} + \widetilde{u_j''}\frac{\partial \overline{p}}{\partial x_i}]$$

$$\epsilon_{ij} = \text{Dissipation Tensor} = \mu\overline{[S_{ik}\frac{\partial u_j''}{\partial x_k} + S_{jk}\frac{\partial u_i''}{\partial x_k}]}$$

Terms in Turbulent Kinetic Energy Equation

$$P_k = \text{Production Term} = -\overline{\rho}\widetilde{u_i''u_j''}\frac{\partial \tilde{u}_i}{\partial x_j}$$

$$D_k = \text{Diffusion Term} = -\frac{\partial}{\partial x_j}(\overline{\rho}\widetilde{u_j''k} + \overline{u_i''p'}) + \frac{\partial}{\partial x_j}(\mu\overline{S_{ij}u_i''})$$

$$C_k = \text{Compressibility Term} = \overline{p'\frac{\partial u_k''}{\partial x_k}} - \frac{\overline{\rho'u_k''}}{\overline{\rho}}\frac{\partial \overline{P}}{\partial x_k}$$

$$\epsilon = \text{Energy Dissipation} = \mu\overline{[S_{ij}\frac{\partial u_i''}{\partial x_j}]}$$

Table 1. Mathematical Forms of Reynolds Stress and Kinetic Energy Equation

where P_k, C_k and ε are the contractions of their corresponding terms. With this algebraic form the cost effectiveness of just using a kinetic energy equation, rather than the six Reynolds-Stress field equations, is reduced. The kinetic energy equation is obtained by contracting the Reynolds stress equation and the modeled ε equation as follows:

$$\frac{Dk}{Dt} = P_k + D_k + C_k - \varepsilon \tag{13}$$

The Algebraic Stress model has considerable appeal, as it offers the advantage of the Reynolds Stress model that is, all effects that enter the transport equations for $\overline{\rho u_i'' u_j''}$ through the source terms, such as body forces (rotations, streamline curvature, buoyancy), anisotropic strain field, high order compressibility, and wall damping influence, can be incorporated. On the other hand, instead of solving six extra partial difference equations, only six algebraic equations must be solved. The resulting model is much more reasonable for application than the Reynolds Stress model and eliminates some uncertainties, associated with assigning proper boundary conditions for the Reynolds stresses. However, this model relies on many of the closure assumptions used for Reynolds Stress Models. Hence, only by properly validating the closure involving D_{ij}, C_{ij}, D_{ij} and π_{ij} terms, can we have confidence in the simpler models which are derived from it.

For non-equilibrium models, at least one of the characteristic scales was estimated by a transport equation to account for the history effects. In most cases, the characteristic turbulence velocity scale is estimated from taking the square root of the turbulent kinetic energy which is governed by equation (13). The characteristic length scale is then determined from a combination of the turbulent kinetic energy and the other scalar turbulence quantity. The turbulence kinetic energy dissipation rate ε and the mean square root of vorticity ω' seem to be most popular choices for length-scale determining transport equations from many other choices[9,12]. The equation for ε can also be derived from the original instantaneous Navier-Stokes equation. However, the more important issue is the interpretation of ε. By definition, the destruction of turbulent energy by viscous action occurs at the finest scale of the fluctuation and is locally isotropic. Using this quantity to determine the characteristic length scale for momentum mixing, which reflects essentially the large-eddy motions, relies heavily on the assumptions of the energy "cascade" process[8]. That is, the turbulence energy dissipation rate is controlled by the rate, at which energy cascades from large to small scale eddies. Thus, the "modeled" transport equation for ε depends heavily on the analogy of the corresponding turbulent kinetic energy equation. The form most frequently used is

$$\frac{D}{Dt}(\bar{\rho}\varepsilon)=\frac{\partial}{\partial x_k}\left(\frac{\mu}{\sigma_\varepsilon}\frac{\partial\varepsilon}{\partial x_k}\right)+C_1\bar{\rho}\frac{\varepsilon}{k}P_k-C_2\bar{\rho}\frac{\varepsilon^2}{k}+\text{Compressibility Effects} \tag{15}$$

The resultant transport equations are also highly sensitive to the model constants C_1 and C_2. For example, a change of C_1 by one percent would decrease the predicted speading rate of a subsonic round jet by as much as 5%. The calculation of the length-scale governing equation itself is probably the weakest link in this level of modeling and may ultimately force an adoption of multipoint methods. Other two-equation models are the $k-\omega^2$ model of Wilcox and Rubesin[9], or the $k^{1/2}-\omega$ model of Coakley[17] and Bardina[11], where $1/\omega$ is related to the characteristic eddy life time k/ω. Experience with the two-equation models indicate the inability of all models to adequately predict the extent of separation caused by shock/boundary layer interaction. Some improvement is obtained by introducing a compressibility correction in the original incompressible version of the $k-\varepsilon$ model, simply by changing the constant that multiplied the dilation terms[18] or by making the model constant Mach number dependable on some ad hoc assumptions[13].

The major task of the Algebraic Stress Model is to model the unknown terms on the right hand side of equation(12). Specifically the pressure strain tensor π_{ij}, which controls the redistribution of turbulent energy among the normal stresses through the interaction of pressure and the strain rate, and the viscous dissipation tensor ε_{ij}. The pressure strain term is modeled through three mechanisms: π_{ij1} resulting from purely turbulence interactions known as "return-to -isotropy"[19], π_{ij2} involving interactions between the mean strain rate and turbulence, the so-called "rapid term", and π_{ijw} relating the effects of solid boundaries on both π_{ij1} and π_{ij2}.

In the present study, the most frequently used linear model of Rotta [19] is adopted for the return-to-isotropy:

$$\pi_{ij1} = -C_1 \frac{\varepsilon}{k}(\overline{\rho u_i'' u_j''} - \frac{2}{3}\delta_{ij}k) \tag{15}$$

More complicated non-linear models, such as the models of [2,20], have been proposed, however, these have shown no significant improvement over Rotta's model. The rapid term is approximated by the isotropization production (IP) model, suggested by Launder[21], thus:

$$\pi_{ij2} = -C_2(P_{ij} - \frac{2}{3}\delta_{ij}P_k) \tag{16}$$

in which

$$P_k = \frac{1}{2}P_{ii}$$

Finally, the dissipation tensor is modeled by

$$\varepsilon_{ij} = \frac{2}{3}\delta_{ij}\varepsilon \tag{17}$$

where ε is the turbulent energy dissipation rate that can be obtained from equation(11).

With these models, the final formulation of eq.(12) results in:

$$\frac{\overline{\rho u_i'' u_j''}}{k} - \frac{2}{3}\delta_{ij} = \frac{1 - C_2}{(C_1 - 1)\varepsilon + P_k}(P_{ij} - \frac{2}{3}\delta_{ij}P_k) \tag{18}$$

It should be noted that the left hand side of the equation is a non-dimensional measure of anisotropy of turbulence.

For the term π_{ijw} , various researchers[20,22,23] have developed models, accounting the "echo effect", to damp the normal velocity fluctuation and redistribute its energy to the other two turbulence intensities. Available models for π_{ijw} involve many complicated terms, and it is not clear, how these formulations can be directly applied to complex geometries. To avoid uncertainties due to the boundary effect, we have adopted a composite modeling approach, which implicitly accounts for the near wall effects. In this study, a two-layer approach is implemented. In the fully turbulent region away from wall, the form of the ASM as described above is adopted. In the near wall region, including overlap regions and viscous sublayer, the one equation $k-l$ model is used, with a scalar eddy viscosity in the inner layer, while the influence of extra rates on Reynolds stress distributions are accommodated in the fully turbulent region. The present approach provides improved resolution over the RSM/wall function approach, commonly adopted in the literature[22].

The matching point for this two layer ASM model is chosen as y^+ =200. Within the matching point, the Reynolds stress tensor is calculated from

$$-\overline{\rho u_i'' u_j''} = C_\mu k^{\frac{1}{2}} l_\mu [(\frac{\partial \tilde{u}_i}{\partial x_j} + \frac{\partial \tilde{u}_j}{\partial x_i}) - \frac{2}{3}\delta_{ij}\frac{\partial \tilde{u}_k}{\partial x_k}] - \frac{2}{3}\delta_{ij}\bar{\rho}\tilde{k} \tag{19}$$

in which

$$l_\mu = C_l n[1 - \exp(-\frac{Re_t}{A_\mu}\frac{25}{A^+})] \tag{20}$$

The near wall shear stress damping provided by l_μ implicitly accounts for near wall pressure strain, though it is only appropriately correlated to the viscous damping effects.

Although the nonisotropic stress model of Eq.(18) is used to evaluate turbulent fluxes in the momentum and kinetic energy equations, the gradient diffusion approximation is retained for the turbulent heat flux terms and turbulent mass terms in the energy and species equations. The effective transport coefficients are modeled through the introduction of the turbulent Prandtl number and turbulent Schmidt number. Thus

$$\overline{\rho u_i'' h''} = -\frac{\mu_t}{Pr_t}\frac{\partial \tilde{h}}{\partial x_i} \tag{21}$$

and

$$\overline{\rho u_i'' C''} = -\frac{\mu_t}{Sc_t}\frac{\partial \tilde{C}}{\partial x_i} \tag{22}$$

These turbulent Prandtl and Schmidt numbers are set to a constant value of 0.9 as commonly used in the literature [34].

3. NUMERICAL IMPLEMENTATIONS

The governing equations(6-9) are mapped into a general body fitted coordinate system by the standard transformation formulae[24]. The dependent variable Φ in the general coordinate system can be expressed in a compact form as follows:

$$\frac{\partial}{\partial t}(\rho\Phi) + \frac{\partial}{\partial \xi}(\rho U\Phi) + \frac{\partial}{\partial \eta}(\rho V\Phi) = \frac{\partial}{\partial \xi}[\frac{\Gamma_\Phi}{J}(g_{11}{}^2 + g_{12}{}^2)\frac{\partial \Phi}{\partial \xi}] + \frac{\partial}{\partial \eta}[\frac{\Gamma_\Phi}{J}(g_{21}{}^2 + g_{22}{}^2)\frac{\partial \Phi}{\partial \eta}] + J\, S^\Phi \tag{23}$$

where U, V are the contravariant variables that represent convective fluxes

$$U = g_{11}u + g_{12}v$$

$$V = g_{21}u + g_{22}v$$

and Γ_Φ and S^Φ are the associated diffusivity and source terms for the variable Φ ($=u, v, h, k, \varepsilon$, etc.). The detailed expressions of the source terms and the cross derivative terms due to grid non-orthogonality are available in [25]. These equations are then discretized using a finite difference method, based on the control-volume formulation on a non-staggered grid arrangement for all dependent variables. The velocity-pressure coupling was resolved earlier by the PISOC algorithm in a time-marching fashion. The salient features of the current MAST-2D include: strong conservation form with Cartesian components as dependent variables, colocated grid/variable arrangement, pressure-based PISO-C algorithm, high order Chakravarthy-Osher TVD scheme, and conjugate gradient (CGS) matrix solver. The current numerical method is capable of computing internal and external flows that are laminar, turbulent, separated or attached, incompressible or compressible and requires no smoothing or explicit under-relaxation other than implied by variations in the time step. Table 2 provides an updated list of features and capabilities of the MAST-2D code. Further details on the numerical method are provided in [25].

Equation(18), which represents a nonlinear coupled system, is implemented in the flow solver by lagging the turbulent kinetic energy production terms P by one time-iteration step. The linearized system is then solved at every grid point directly by Gaussian elimination. The final model has been validated for several flows including a compressible developing boundary layer flow, a separated flow,and a swirling flow. A complete thrust chamber flow field calculation has been executed also. The computed results will be discussed below.

Table 2. Updated features of the MAST code.

ORGANIZATION			UAH		
RESPONS. PERSON			C.P. Chen		
CODE NAME			MAST		
DIMENSIONS					
COORDINATES	CART/CYL/SPH/BODY FIT		BdyFit		
TIME PROBLEM	STEADY/UNSTEADY		Unsteady		
TYPE OF FLOW	INVISCID/VISCID	Inviscid, Viscid: Laminar/Turbulent	Invis,Vis(√T)		
	INCOMP/COMPRESSIBLE	Incomp, Comp: Sub/Tran/Super/Hyper	Incomp,Comp(?)	Incomp,Comp(Sub/Tran/Super)	
EQUATIONS	CONSERV/NONCONSERV		Conserv		
	MOMENTUM	N-S(Incomp/Comp),PNS,Euler,etc.	N-S(Incomp/Comp),Eu		
	ENERGY		Yes		
	SPECIES	Max. No. of species handled	Yes(7)	Yes(11)	
	MULTI PHASES TRACKING	Eul-Eul,Eul-Lag, Statistic	E-L,Stat		
	EQUATION OF STATE	Ideal,Real Gas	I.G.,R.G.(Eqn)		
	TRANSPORT PROPERTIES	Viscosity,Conductivity-Table,Equation	Eqn		
PHYSICAL PROCESS	TURBULENCE MODELING	Zero(Mixing Length/Baldwin-Lomax),1-EQ,			
		2-EQ(K-L,KEHigh,KELow,etc.),LES,PDF,	KeH,KeL		
		Algebraic Stress/Reynolds Stress M	Multi-Scale Model	Algebraic stress	
	ATOMIZATION MODEL	Drop Size(Assumed/Calculated),Others	Assmd	Assmd, Calcu	
	VAPORIZATION MODEL	Droplet(Single/Multi),Critical Region(Sub/Sup)	Drplt(S/M),Crit(Sb)		
	CHEMISTRY MODEL	None,Equilibrium,Finite Rate,etc.	EQ	EQ, FR	
	RADIATION MODEL	State Source: Flame,Wall,etc.	.		
ROCKET PROPELLANT	TYPE	O2,H2,Hydrocarbon,Hypergolic,etc.	H2/O2	HC/Air	
	PHASES(FUEL/OX)	Single, Two(Gas,Liquid,Solid)	Two(G/S,G/L)		
DISCRETIZATION	FDM/FVM/FEM/SPECTRAL/ETC.		FVM		
NUMERICAL SCHEME	VARIABLES BASED	Pressure Based,Density Based, Others	P,V		
	DIFF. ACCURACY:TIME/SPATIAL	Time(1st,2nd)/Spatial(1st,2nd,Higher)	T(2nd)/S(2nd)		
	MULTI STEP/FACTORIZATION	MS(Yes,No)/FACT(Yes,No)	MS(Yes)/FACT(No)		
	EXPLICIT	Leap/DuF-Frank,Lax-Wend,MacCormack,etc.			
	IMPLICIT	MacCormack,Beam-Warming,Bailey-McDonald			
	OTHERS: SPECIFY	Crank-Nicolson,ADI,TVD,ALE/ICE-ALE			
		Flux Corrected Transport,Taylor-Galerkin,etc.			
		SIMPLE,PISO,SOLA-VOF,etc.	PISOC		
	MULTIGRID CAPABILITY	Yes/No	Yes		
MATRIX SOLVER	DIRECT METHOD	TDMA,Block TDMA,Ester Vector Prop.,etc.			
	ITERATIVE METHOD	Line Iter.,Gauss-Seidel,SOR,etc.			
GRID		Conjugate Gradient/Residue Method	CGM(CGS)		
	SEPARATE (NAME)	EAGLE,Grid Generation Package,etc.			
	INTERNAL	Stagg./Non-Staggered,Orthog/Non-Orthog.	Nonstag	NS Ort/Nonort	
		Struct/Unstructured,Adaptive Grid,Multi zone			
INLET/WALL	TECHNIC USED	FEM,Algebraic,Differential Eq's	Diff		
BOUNDARY COND.	INLET CONDITIONS	Constant,Time Varying,Characteristic	Const,Time Var		
	WALL BOUNDARY	No slip/Slip,Stationary/Moving	Nslp,MV		
		Adiabatic,Isotherm,Constant Flux,etc.	Const,Time Var		
		Smooth/Rough Surface	Surf(S)		
		Droplet wall interaction(Adhesion/Bounce)	Adh,Bounce		
PROGRAM CAPABILITY (Experienced)	INCOMPRESSIBLE FLOWS	Reynolds No. Ranges	1.0E1 - 1.0E6		
	COMPRESSIBLE FLOWS	Mach No. Ranges	0.1 - 8		
	INTERNAL FLOW	Separating,Recirculating,Cavity Flows,etc.	Separ,Recirc,Cavity		
		Combustion Chamber,Nozzle		Comb, Nozz	
	INJECTION	Element: Coaxial,Impinging	Coax		
		Process: Atomization,Mixing,Vaporization	Vap,Mix		
	PERFORMANCE PREDICTION	Thrust Chamber: Isp,Therm Props,Dynamics		Thrust	
	MISC.	Other than Thrust Chamber			
CODE VALIDATION	UNIQUE CASES	No. Solved(include benchmark cases)	15	25	
	CASES PUBLISHED	Number	10	17	
	THRUST CHMBR RELATED	Number	0	2	
PRE/POST PROCESSOR	DEVELOPED	In-house, By Others	Inhouse		
	OPERATION	Batch,Interactive	Batch		
	GRAPHICS	Display,Plot3D,Self,etc.	Display		
PROGRAM	DOCUMENTATION	Manual-Engineering,Program,User	Eng,Prog		
	AVAILABILITY	Proprietary,Sale,Process(SBIR),Pub. domain	Pub		
COMPUTER SYSTEM	MAIN FRAME	Cray,IBM,Cyber,etc.	Cray		
	MINI COMPUTER	Convex,Alliant,Vax,etc.			
	WORKSTATION	Sun,Apollo,Tek,SiliconG.,etc.	Sun		
MISCELLANEOUS	CODE EXPERIENCE	No. of years Used	Developing		
	CODE ORIGIN	In-house/Acquired: Original code name	Inhouse		
	VECTORIZATION	Programmed for vectorization(Yes/No)	No		

Survey Date: October 1990 (Except ***)

ORIGINAL PAGE IS OF POOR QUALITY

4. RESULTS AND DISCUSSIONS

Boundary Layer Flows

The model, developed in this study, is used first to calculate compressible flat plate boundary layers on adiabatic as well as cooled walls, and the results are compared with benchmark experimental data of [26, 27]. The calculations were carried out over the Mach number range, 0<Ma<5, for the adiabatic wall condition and over the temperature range, 0.2<Tw/Taw<1, for the cool wall case. Here, Ma is the free stream Mach number , Tw is the prescribed wall temperature, and Taw is the adiabatic wall temperature. Calculations were done by either direct integration to the wall, using the damping functions described above or integration to the inertia sublayer, using the wall function. In Figure 1, the normalized skin frictions, predicted by the ASM and the two-equation $k-\varepsilon$ model are compared with the Van Driest curve and experimental data for a range of external Mach numbers.The current ASM model gives even better predictions, compared to the recent compressibility-corrected k-e model predictions [28], and is also in good agreement with the full Reynolds Stress Closure results [30]. The predictions for the cooled wall are shown in Figure 2. As pointed out by [29], if the cooled-wall flows are to be predicted correctly, turbulent heat fluxes and their near-wall behavior need to be realistically modeled. The current two-layer approach appears to model these aspects satisfactorily. In Figure 3, the near wall mean velocity profiles are plotted in terms of wall parameters, based on friction velocity, wall shear stresses and molecular viscosity. The calculated profiles based on the ASM/two-layer model are in agreement with data over a wide range of y+. The slope of the calculated profiles are also roughly parallel to that determined from measurements. The predictions of the near wall flow can be further examined from the profiles of the normalized kinetic energy and the normalized Reynolds stress in Figures 4a and 4b. These results are consistent with the asymptotic analytical results deduced from the direct numerical simulation calculations [29].

2-D Backward-Facing Step Flow

The second test case is the two-dimensional backward-facing step flow, involving massive flow separation. The experimental data of Driver and Seegmiller [31] was used for comparison. The treatment of this problem follows closely the procedure described in [25]. Thus, only the relevant second order results are presented here. The predicted values of the reattachment length of the recirculation zone behind the step, using the $k-\varepsilon$ model and the ASM closure, are 4.76 and 5.94 step heights respectively. The reported experimental data on the reattachment length is about 6.1 with some fluctuations of about a 0.2 step height. The current ASM model performs much better than the eddy-viscosity $k-\varepsilon$ model for recirculating flows. In terms of turbulence quantities, comparisons of the predicted streamwise and lateral turbulence intensities, as well as the Reynolds stress component obtained from the solutions of ASM Eq. (18), and estimates from the constitutive equation (10) by using the $k-\varepsilon$ model, are shown in Figure 5. The results were normalized with the inlet centerline velocity. The non-isotropic imbalance of the turbulence intensities as well as the level of Reynolds stress are much better predicted by the ASM closure.

Confined Swirling Jet Flow

The next case involves flows with separations and streamline curvature due to swirl. The confined swirling jet, experimentally carried out by Roebuck and Johnson [32],is chosen for the model assessment study. The swirl number, S, obtained from the experimental data, is 0.375. In a coaxial swirling jet, the swirl number is defined as $S = \dfrac{\int_0^R \rho UWr\, dr}{R\int_0^R \rho U^2 r\, dr}$,in which U is the mean axial velocity W is the tangential mean velocity, and R is the annular jet radius. The inlet boundary conditions were set at 5mm downstream of the jet exit, at which the measured quantities in terms of mean and turbulence quantities are available. The results are obtained on a 81x81 non-uniform mesh with refinement in the recirculation regions and the entrance region. Grid independence was confirmed by performing another calculations with 101x101 grid cells. The difference between the two results is within 2%.

Figure 6 shows comparisons of the axial velocity along the centerline using the ASM closure and the two-equation model. In terms of the strength and location of the centerline reversal velocity, the ASM model yields better agreement than the $k-\varepsilon$ model. Comparisons of the predicted mean axial and tangential velocity profiles with experimental data are presented in Figure 7a and 7b. Both models show favorable agreements in the axial velocity profiles, but slight deviations in the radial components downstream. The good predictions obtained by the $k-\varepsilon$ model, which are in contrast to previous results in the literature, are mainly related to the second order difference scheme used in the present MAST code, and partly due to the relatively low swirl number situation. However, both models predict the rapid decay of tangential velocity to a solid-body rotation at the downstream locations.The cauculated tangential velocity recovers too quickly to the ultimate forced-vortex structure of confined swirling flows. This points to the deficiency of the ASM assumptions in which the "advection" of Reynolds stresses responds too quickly to the turbulent kinetic energy. The full differential RSM probably has to be used to correctly account for the history of turbulent momentum transport, which ultimately may slow down the recovery of the swirl velocity [35].

Comparisons of turbulent intensities and Reynolds stresses are shown in Figure 8a and 8b. The predicted results of the two models qualitatively follow the trend of experimental data. In terms of the detailed profiles of turbulence properties, the ASM model conforms fairly well to the experimental data, while the $k-\varepsilon$ model predicts some relatively large deviations, especially, in the upstream region, where the non-isotropic turbulence prevails. The basic shortcomings of the $k-\varepsilon$ model for which the isotropic eddy viscosity assumption is employed indicates the inability to redistribute the Reynolds stresses.

SSME Nozzle

The geometry and chamber conditions follow the specifications used in [33]. The flow is subsonic at the inlet and supersonic at the nozzle outlet. A 81x71 grid with a very fine grid cluster near the nozzle wall was used to resolve detailed boundary layer flow structures.

Both the $k-\varepsilon$/two-layer and the ASM/two-layer model were used for comparison purposes. Figure 9(a,b) show the iso-Mach lines of the non-reacting flow fields inside the nozzle. Figure 10(a,b) show the temperature contours. The difference between these two predictions is very small in terms of overall flow properties. The specific impulse of 100% power level is calculated as 513.53 seconds using the $k-\varepsilon$/ model and is 513.79 using the ASM. The noted difference is in the predictions of turbulent quantities, such as the kinetic energy level, plotted in Figure 11, for the near wall region at the nozzle exit. The different kinetic energy levels may have some impact on the near wall turbulent structure at the nozzle exit.

This aspect can be investigated by carrying out a detailed calculation for the exit flow around the nozzle exit manifold. Geometry of the nozzle manifold is shown in Figure 12 [34]. Detailed temperature profiles along the nozzle wall was also supplied by Mr. Gross. The grids used for this calculation are shown in Figure 13(a) and (b). The calculated flow field characteristics from a previous whole SSME nozzle solution were used as inlet boundary conditions for the domain of interest. Specifically, the calculated profiles at the axial location x=117 [inches] from the nozzle throat were used. The boundary conditions away from wall were selected to ensure supersonic boundary conditions.. At the outer boundary for the calculation domain, either specified total pressure (for subsonic regions) or extrapolated boundary conditions (for supersonic regions) are specified. Two-layer treatment of the turbulence quantities as well as non-slip, isothermal boundary conditions were used at the wall.

A 81x51 grid with about 15 grid points covering the near-wall inertia sublayer (y^+ <50) was used for the calculations. The external total pressure was set to 1 Atm. The calculated flow fields, using the ASM model, were shown in Figure 14,15,16 in terms of Mach number contours, pressure contours, and vector plots. It is evident that a shock-boundary layer interaction is experienced near the exit lip of the changing wall geometry. Due to the entrainment of external air, two recirculation bubbles are formed behind the oblique shock. A supersonic pocket region is also observed near the manifol exit due to the entrainment. Static pressures along the wall are plotted in Figure 17(a) and (b) using the two different turbulence models. Effects of wall temperatures are also shown. It can be seen that the $k-\varepsilon$ model moves the shock location slightly toward the nozzle exit and produces a lower pressure after the jump. The lower wall temperature also produced the same effect as the $k-\varepsilon$ by comparison to the ASM model.

To investigate the effect of chamber pressure, another calculation was performed with a reduction in chamber pressure by 25% . From the pressure contour shown in Figure 18, the shock moved further inside the nozzle. The boundary layer around the shock region is still very thin. No analytical flow separation was observed. The final run involved molecular viscosity only, to simulate laminar flow. The boundary layer thickened and pushed the shock location upstream significantly as seen in Figure 19. However, still no flow separation was observed ahead of the shock formation.

5. CONCLUSIONS AND RECOMMENDATIONS

In this study, an Algebraic Stress Model (ASM) coupled with a two-layer near-wall treatment was developed and successfully implemented into the MAST code. To validate the model and the numerical implementation, a series of test case ranging from compressible flat plate flows, a recirculating flow, a confined swirling flow were computed and the results were compared with the base-line $k-\varepsilon$ model and available experimental data. Further applications including the entire SSME nozzle flow and the SSME exit wall flow around the nozzle manifold were studied. For recirculating flows and swirling flows, the ASM model shows improved results, compared to the $k-\varepsilon$ model, due to its ability to account for the non-isotropic effects. For SSME nozzle flow and exit flows around the nozzle manifold, the effects of second-order turbulence closure do not show significant difference from the two-equation model calculations. The flow fields are dominated by shock/boundary layer interactions coupled with air entrainments from the outer boundaries.

There are few suggestions for future work. First, the full Reynolds Stress Model (RSM) should be incorporated. One of the key difficulties in implementing the RSM is the specification of boundary conditions for Reynolds stresses and the near wall damping models. The two-layer model used in this study coupled with the ASM can be readily extended for RSM implementations. The RSM accounts for the history as well as transport of second-order stresses, which may better resolve detailed chock-boundary layer interactions. Second, the second-order closures should be implemented in three-dimensional numerical models to better resolve three dimensional effects. Third, the second order closure in terms of passive scalar transport such as turbulent heat fluxes (correlation of velocity fluctuation and velocity fluctuation) and turbulent mass fluxes (correlation between concentration fluctuation and velocity fluctuation) should be developed to better simulate mixing and combustion processes in thrust chamber.

References:

1. Rubesin, M. W., "Turbulence Modeling for Aerodynamic Flows", AIAA Paper 89-0606, 1989.

2. Kline,S. J., Cantwell, B.J. and Lilley, G. M., The 1980-81 AFORS-HTTM-Stanford Conference on Complex Turbulent Flows, Stanford University, 1982.

3. Favre, A., " Equations for Compressible Turbulent Gases", J. Mechanics, Vol. 4, p. 361,1965.

4. Rodi, W., " A New Algebraic Relation for Calculating the Reynolds Stresses", ZAMM.,Vol. 56, p. 219, 1976.

5. Cebeci, T. and Smith, A. M. O., "Analysis of Turbulent Boundary Layers", Academic Press, 1974.

6. Baldwin, B. and Lomax, H., "Thin Layer Approximation and Algebraic Model for Separated Turbulent Flows", AIAA Paper 78-257, 1978.

7. McDonald, H. and Camarata, F. J., "An Extended Mixing Length Approach for Computing the Turbulent Boundary Layer Development", Proceeding, Stanford Conference on Turbulent Boundary Layers, Stanford University, p. 83, 1969.

8. Tennekes, H. and Lumley, J. L., "A First Course in Turbulence", MIT Press, 1972.

9. Wilcox, D. C. and Rubesin, M. W., "Progress in Turbulence Modeling for Complex Flows Fields Including Effects of Compressibility", NASA TP-1517, 1980.

10. Coakley, T. J., "Turbulence Modeling Methods for the Compressible Navier-Stokes Equations", AIAA 83-1693, 1983.

11. Bardina, J., "Toward a General Turbulence Model", AIAA Paper 89-1862, 1989.

12. Jones, W. P. and Launder, B. E., "The Prediction of Laminarization with a Two-Equation Model of Turbulence", Int. J. Heat and Mass Tran., Vol. 15, p. 303, 1972.

13. Morel, T. and Mansour, N. N., SAE Paper No. 820040,1982.

14. Jones, W. P. and Whitelaw, J. H., " Calculation Method for Reacting Turbulent Flows: a Review", Comb. and Flame, Vol.48, p. 1, 1982.

15. Johnson, B. V. and Bennet, J. C., " Mass and Momentum Turbulent Transport Experiments with Confined Coaxial Jets", NASA CR-165574, 1981.

16. Workshop on Turbulence Modeling for Liquid Rocket Thrust Chamber, April 15-16, UAH,1991.

17. Coakley ,T . J., " Turbulence Modeling for the Compressible Navier-Stokes Equations", AIAA Paper 83-1693,1983

18. Viegas, J. R and Rubesin M.W., "A Comparative Study of Several Compressibility Corrections to Turbulence Models Applied to High Speed Shear Layers", AIAA Paper 91-1783,1991

19. Rotta, J. C. "Statistische Theorie nichthomogener Turbulenz", Z. Physik, Vol. 129, 547,1951

20. Lumley , J. L. and Khajeh-Nouri, B. J., " Computational Modeling of Turbulent Transport", Adv. Geophys., Vol. 18A, 169, 1974.

21. Launder, B. E., "Second Moment Closure and Its Use in Modeling Turbulent Industrial Flows", Int.Num. Meth. Fl., Vol. 9, 963, 1989

22. Shih, T. H. and Lumley J. L., "Second Order Modeling of Near-Wall Turbulence", Physics of Fluids, Vol. 14, 971,1986

23. Launder , B. E., Reese , G. J. and Rodi, W., " Progress in the Development of a Renolds Stress Closure", J. Fluid Mech. Vol. 68, 537,1975

24. D.A. Anderson, J.C. Tannehill and R.H. Pletcher, Computational Fluid Mechanics and Heat Transfer, Hemisphere Pub. N.Y., 1984

25. C.P. Chen et. al. "A Computer Code for Multiphase All-Speed Transient Flows in Complex Geometries, MAST Version 1.0" , October,1991

26. H. H. Fernholz and P. J. Finley, "A Critical Compilation of Compressible Turbulent Boundary Layer Data," AGARD, No, 233, 1977.

27. S. J. Kline et al., Proceedings of the 1980-1981 AFOSR-HTTM-Stanford Conference on Complex Turbulent Flows, Stanford U. Press, CA, 1981.

28. S. Sarkar, G. Erlebacher, M. Y. Hussaini and H. O. Kreiss, "The Analysis and Modeling of Dilatational Terms in Compressible Turbulence", ICASE Report 89-79, Hampton, VA, 1989.

29. H.S. Zhang, R.M.C. So, Speziale C. G. and Y. G. Lai, "A New-Wall Two-Equation Model for Compressible Turbulent Flows", AIAA 92-0442, 1992.

30. C. G. Speziale and S. Sarkar, "Second-Order Closure Models for Supersonic Turbulent Flows", AIAA Paper 91-0217, 1991.

31. D. M. Driver and H. L. Seegmiller, "Features of a reattaching turbulent shear layer in divergent channel flow", AIAA J., Vol. 23, pp163-171, 1985.

32. R. Roback and B.V. Johnson, "Mass and Momentum Turbulent Transport Experiments with Confined Swirling Coaxial Jets," NASA CR-168252, 1983.

33. T. S. Wang and Y. S. Chen, "A Unified Navier-Stokes Flowfield and Performance Analysis of Liquid Rocket Engines," AIAA Paper 90-2494.

34. R. Srinivasan, R. Reynolds, I. Ball, R. Berry, K. Johnson and H. Mongia, "Aerothermal Modeling Program," Final Report, NASA CR-168243, 1983.

35. B. Lakshminarayana, "Turbulence Modeling for Complex Shear Flow," AIAA J. Vol. 24, No.12, 1986.

36. K.W. Gross, Private Communication.

37. C. P. Chen, et al., "A Computer Code for Multi-Phase All-Speed Transient Flows in Complex Geometries, MAST Version 1.0", October, 1991.

38. C. P. Chen and S. T.Wu, "Development of Generalized Pressure-Velocity Coupling Scheme for the Analysis of Compressible and Incompressible Combusting Flows", Final Report for NASA NAG8-128, December, 1992.

Appendix 1

Publications Resulting From This Contract

1. Kim Y. M., Shang H. M. and Chen C. P., "Non-Isotropic Turbulence Effects on Spray Combustion", 27th Joint Propulsion Meeting, AIAA paper 91-2196, 1991.

2. Kim Y. M., Chen C. P. and Shang H. M., "Predictions of Confined Swirling Spray-Combusting Flows Using a Non-Isotropic Turbrlence Model", acceped for publication, Int. J. Numerical Heat Transfer, 1992.

3. Shang H. M., Chen C. P. and Huang J., "Predictions of Supersonic Shear Flows using a Hybrid ASM/Two-Layer Model", 29th Joint Propulsion Meeting, Montarey, CA, 1993.

4. Huang J., "Assessment of an Algebraic Stress Model for Compressible Flows", M.S. Thesis, to be completed, May, 1993.

Appendix 2
Sample Inputs

The MAST family computer programs consists of a set of subroutines controlled by a short main program. The fundamental structure can be found in the MAST user's manual version 1.0 [37]. The updated capabilities, resulting from a previous study, were summarized in [38] for the version 1.1. Sample inputs for calculations of SSME thrust chamber flows and nozzle outlet manifold flows are given in Table A.1 and A.2. To activate the usage of the Algebraic Stress Model, keyword ASM is added in the TURBULEN Block as seen from Table A.1 and A.2.

```
CONTROL    COMPRES NCRT 3   OMGM 1   NCGM 50
           OMGD 1.0 PHI -1 OMGPHI 0.00  OMGT 0.50 OMGF 1.00
           ERRCG 1.0E-2 ERRM 1.0E-5 IMON    81 JMON 10 MONU
;RESTART
GRID  NX    81   NY   71   AXISYM   READXY
BOUND
    IST   1  IEND     1  JST  1  JEND  71  INLET IPBC 3
    IST   1  IEND    81  JST 71  JEND  71  WALL U 0 V 0 TK 0 IPBC 3
    IST   1  IEND    81  JST  1  JEND   1  SYMMETRY IPBC 3
    IST  81 IEND     81  JST  1  JEND  71  OUTLET   IPBC 3
TURBULENT   TKIN 3. TEIN 1.E4      ASM
PROPERTY VISCOS    -1 ; CALCULATE BY SUTHERLAND'S LAW
        PSTAG 20240946.90  TSTAG 3637.   GAMMA 1.2  GMW 10.18
SOLV  U     V  P  TEMP    TK  TE
RUN    DT 1.E-7 DTMIN   2.E-7 DTMAX 2.E-5   CFLN 1.00 NSTEP 4000
       NPR1 1    NPR2 100    NEX 18
ENDJOB
```

Table A.1. Input file of the whole SSME calculation using ASM model

```
CONTROL    COMPRES NCRT 3   OMGM 0   NCGM 50
           OMGD 1.0 PHI -1 OMGPHI 0.30  OMGT 0.30 OMGF 1.00
           ERRCG 1.0E-2 ERRM 3.0E-5 IMON    81 JMON 10 MONU
;RESTART
GRID  NX    81   NY   51   AXISYM   READXY
BOUND
    IST 1   IEND 1    JST   1  JEND  51  INLET IPBC 1
    IST 1   IEND 81   JST  51  JEND  51  WALL U 0 V 0 TK 0 IPBC 3 TEMP 300.
    IST 1   IEND 81   JST   1  JEND   1  OUTLET    IPBC 2
    IST 81  IEND 81   JST   1  JEND  51  OUTLET    IPBC 2
TURBULENT   TKIN 3. TEIN 1.E4      ASM
PROPERTY PREMAX 1.2E+5 PBACK 1.E+5
       VISCOS   -1 ;VISCOSITY IS CALCULATED BY SUTHERLAND'S LAW
       PIN 1.E+5   TIN 300.  GAMMA 1.2   GMW 10.18
SOLV  U     V  P  TEMP    TK  TE
RUN    DT 5.00E-7 DTMIN    5.E-7 DTMAX 5.E-5  CFLN 1.00 NSTEP 4500
       NPR1 10 NPR2 100      NEX 20
ENDJOB
```

Table A.2. Input file of the SSME exit flow using ASM model

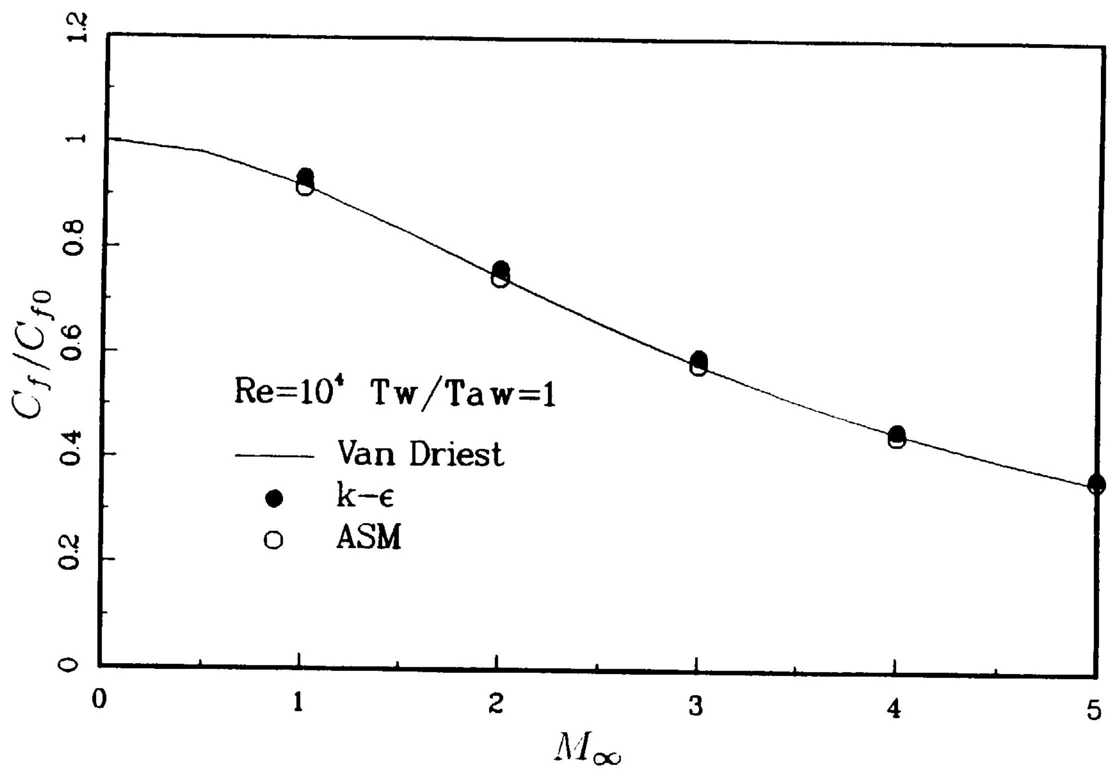

Fig. 1 Variation of C_f/C_{f0} with M_∞ for adiabatic wall boundary condition.

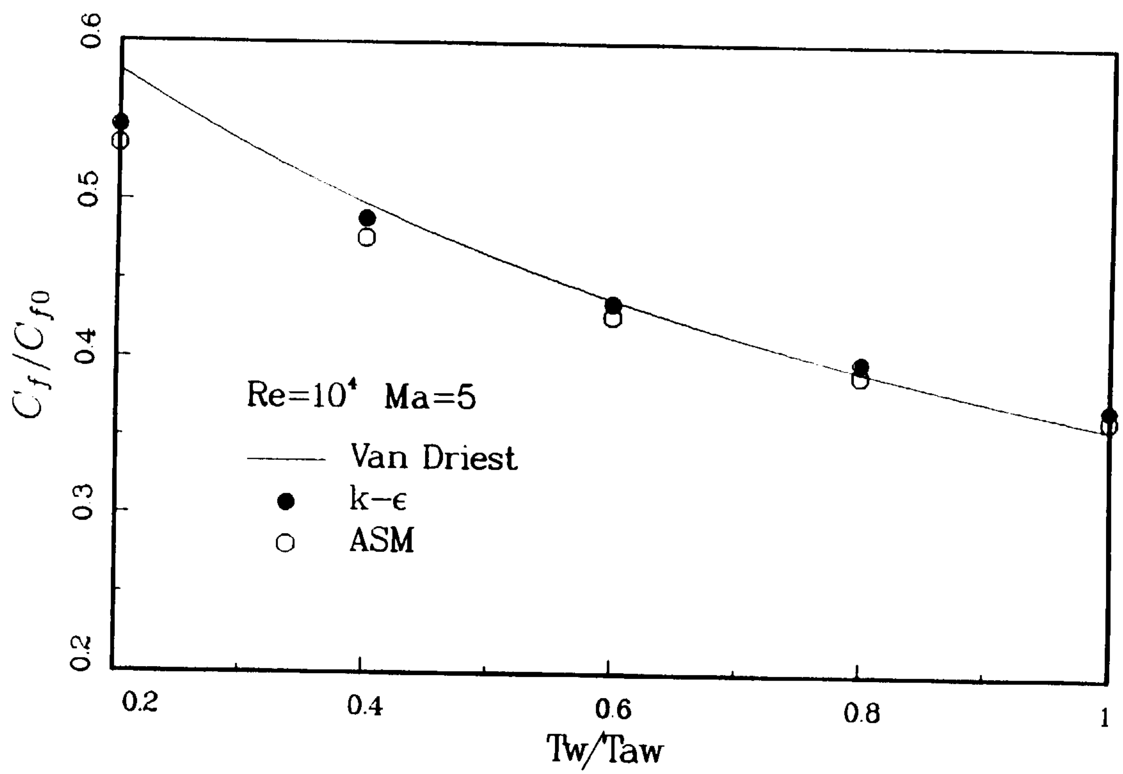

Fig. 2 **Variation of C_f/C_{f0} with T_w/T_{aw} for $M_\infty = 5.0$.**

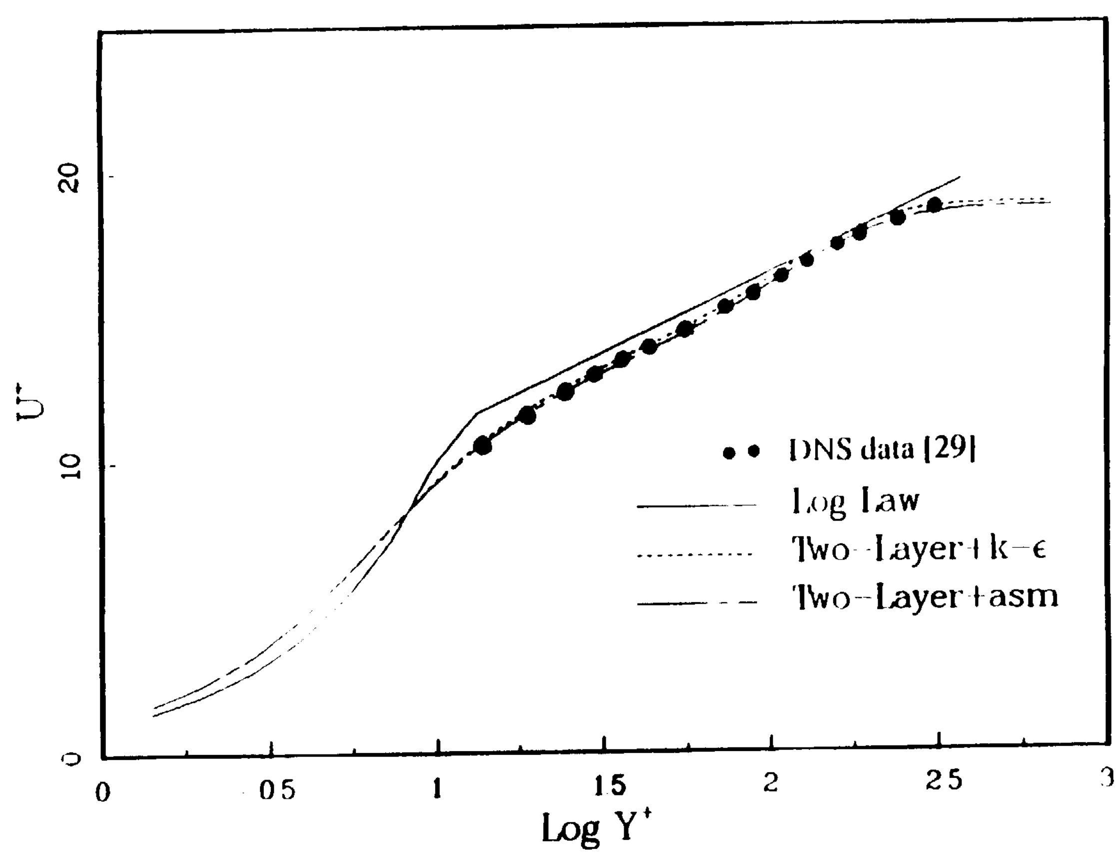

Fig. 3 Semi-log plots of u_c^+ for adiabatic wall boundary condition.

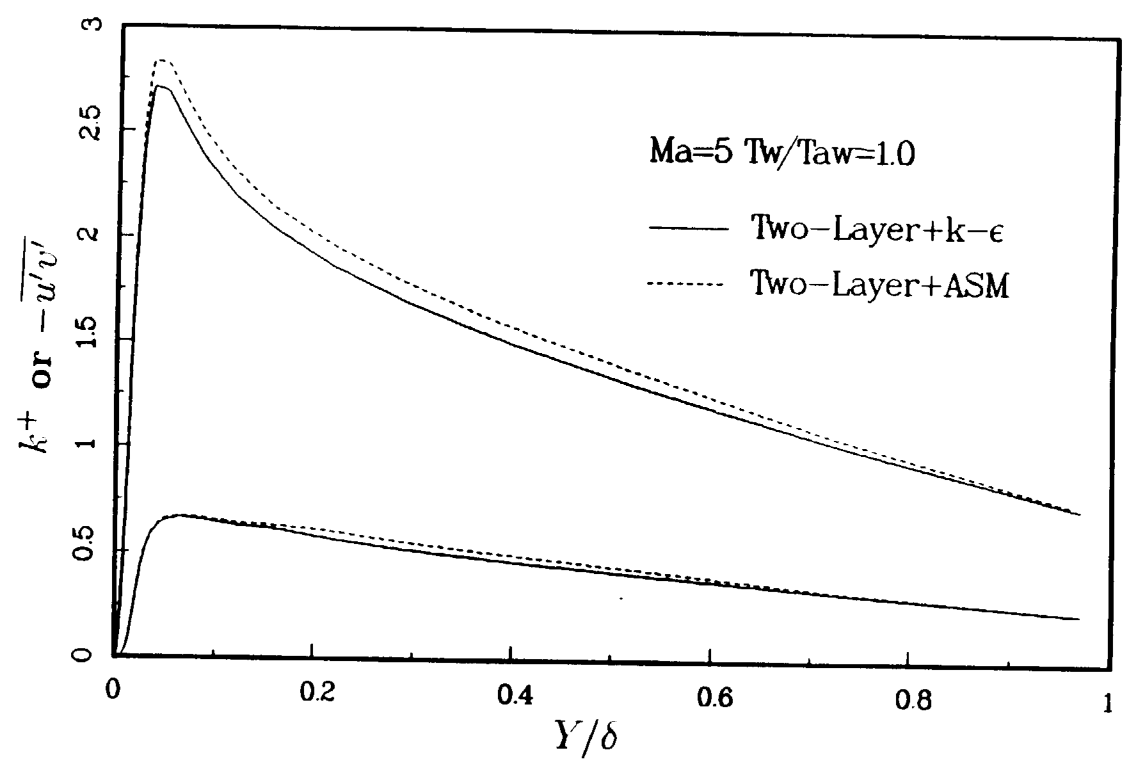

Fig. 4a Behaviors of k^+ and $\overline{u'v'}$ across the boundary layer for adiabatic wall boundary condition.

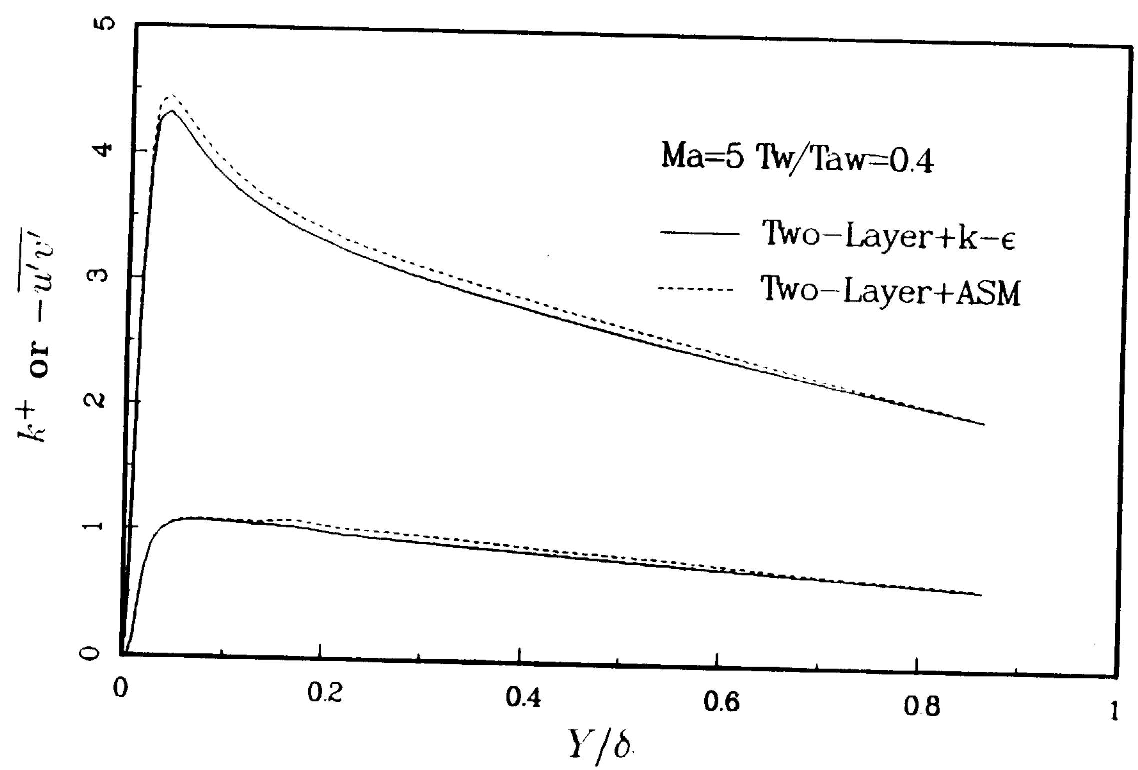

Fig. 4b Behaviors of k^+ and $\overline{u'v'}$ across the boundary layer for cold wall boundary condition ($T_w/T_{aw} = 0.4$).

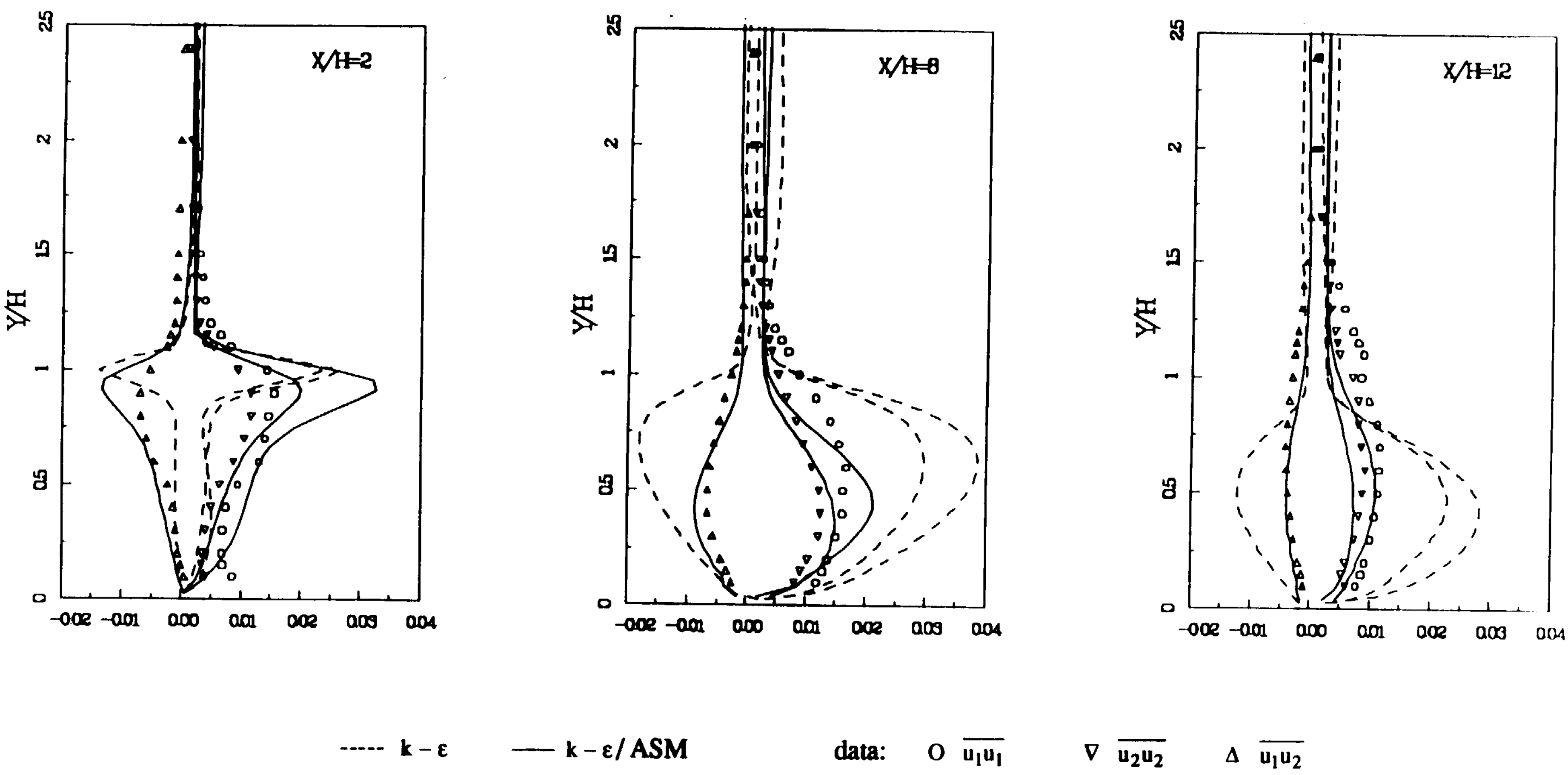

Fig. 5 Reynolds stress profiles for the backward-facing step turbulent flow (9:1), with data from [31]

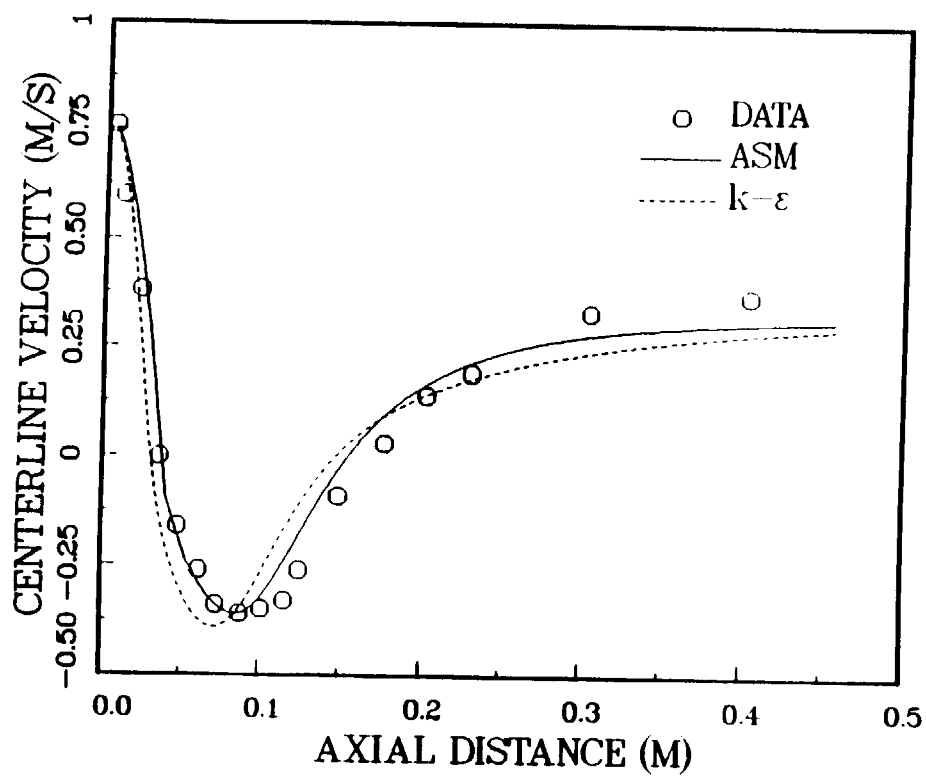

Fig. 6 Decay of mean axial centerline velocity.

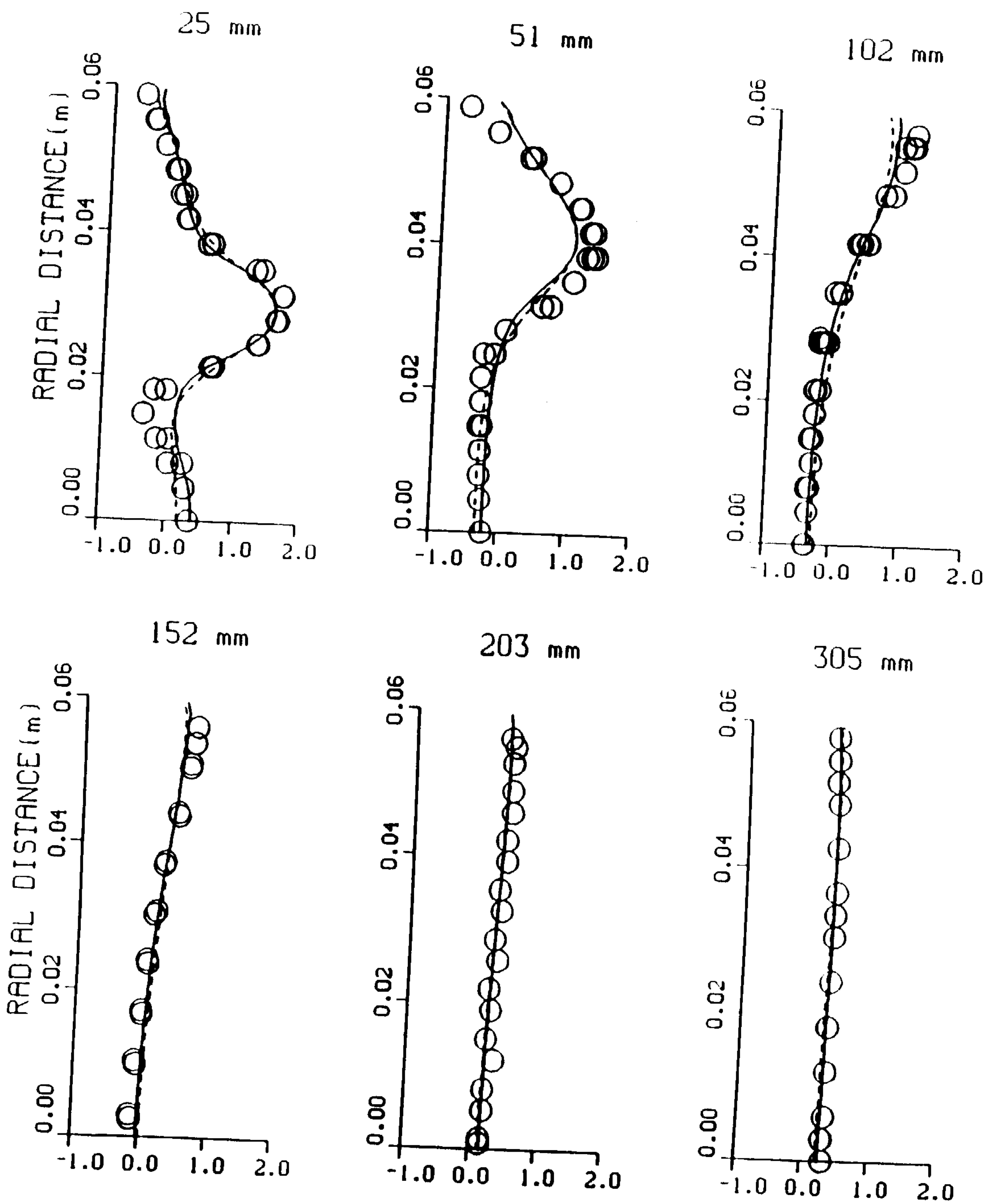

Fig. 7a Radial profiles of mean axial velocity

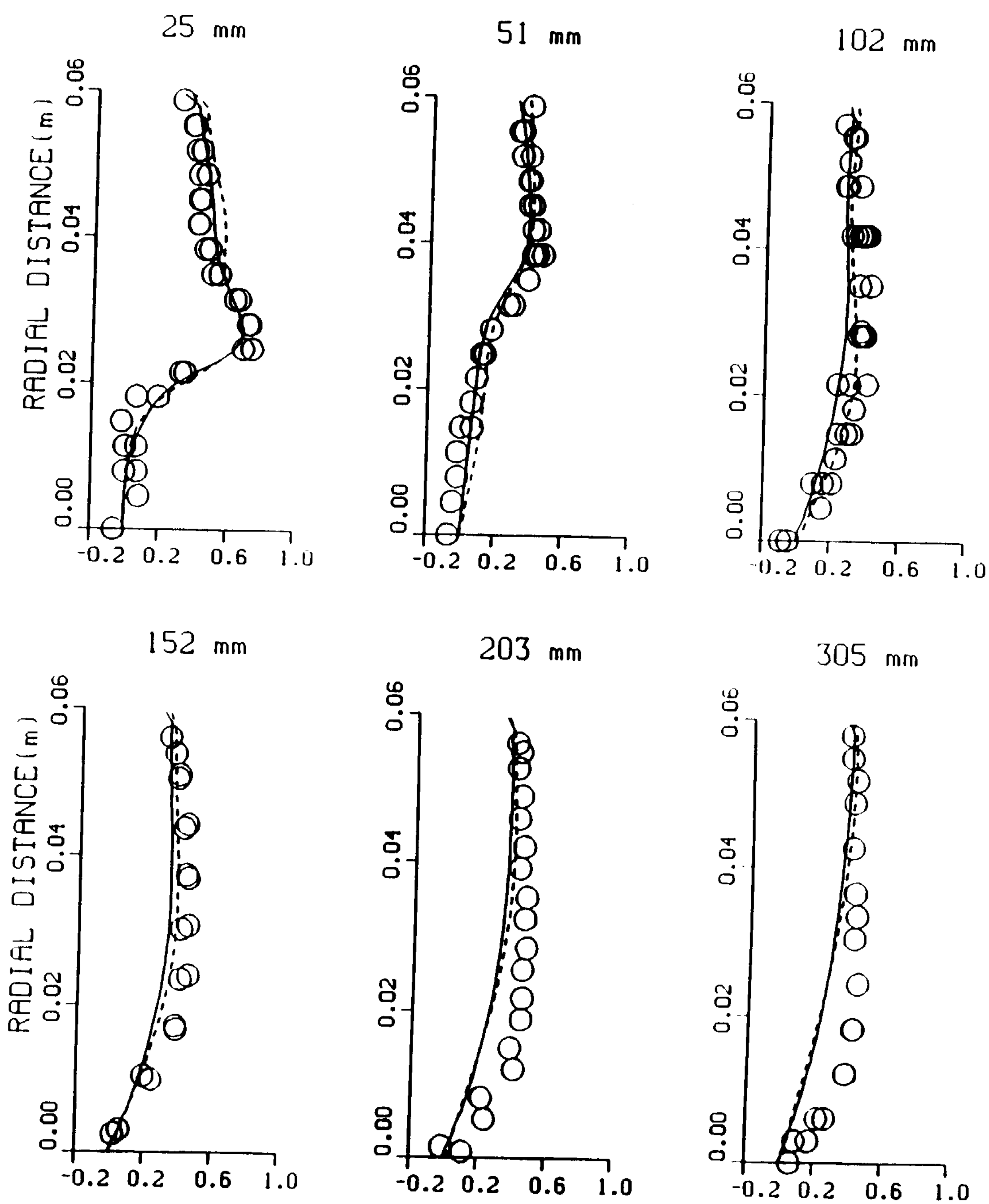

Fig. 7b Radial profiles of mean tangential velocity

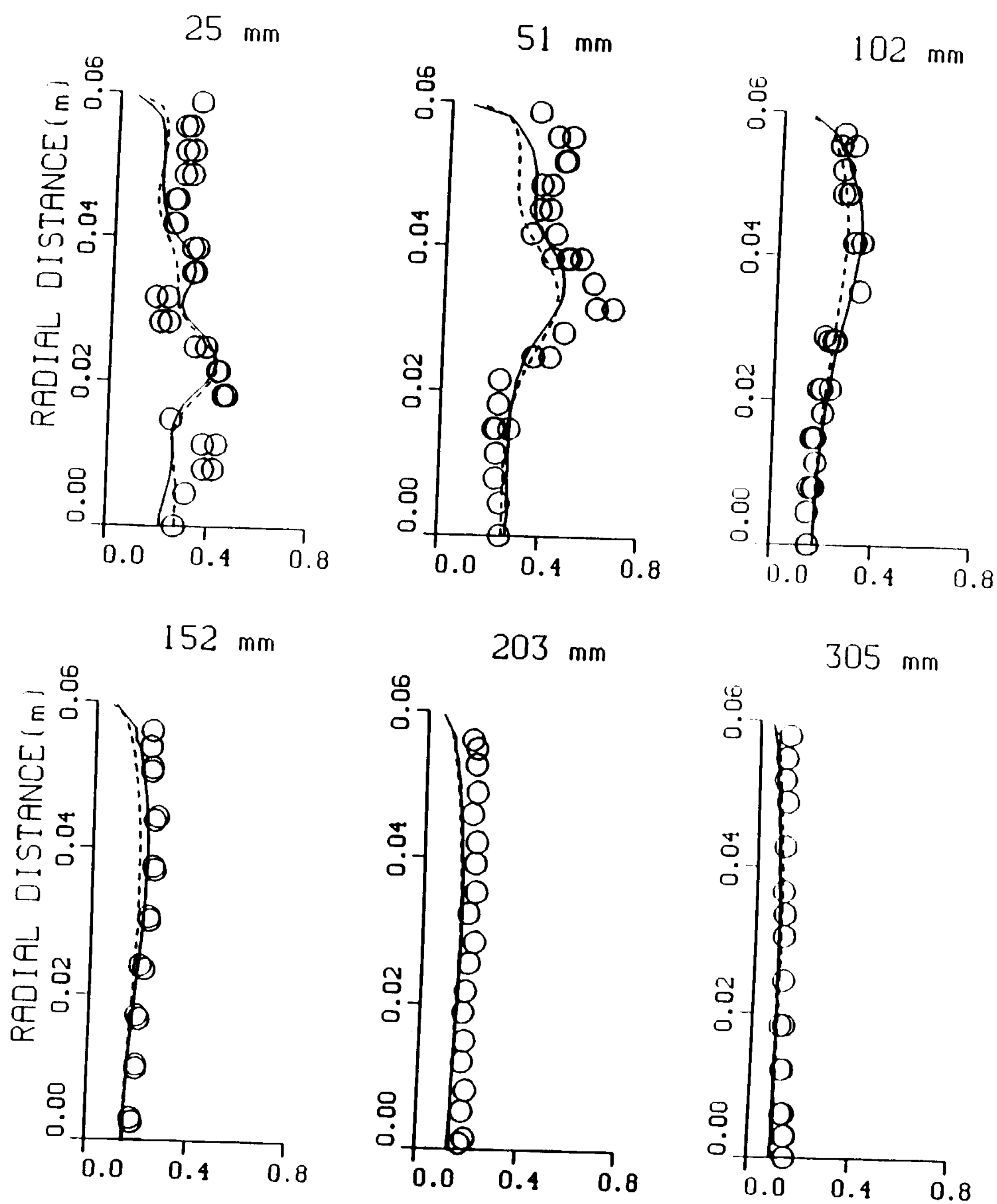

Fig. 8a Radial profiles of turbulent intensity($\sqrt{\overline{u'^2}}$)

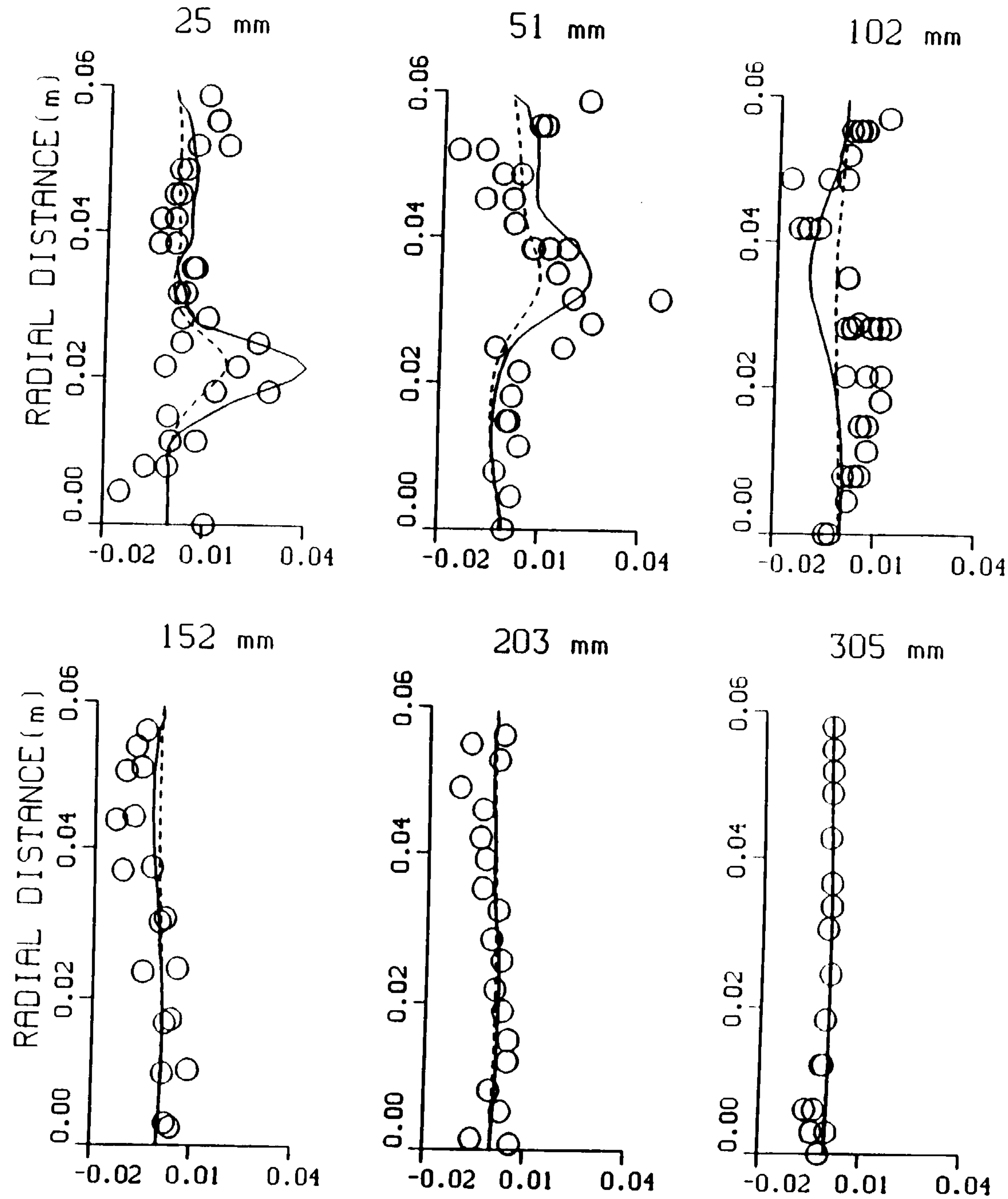

Fig. 8b Radial profiles of Reynolds stress($\overline{u'w'}$)

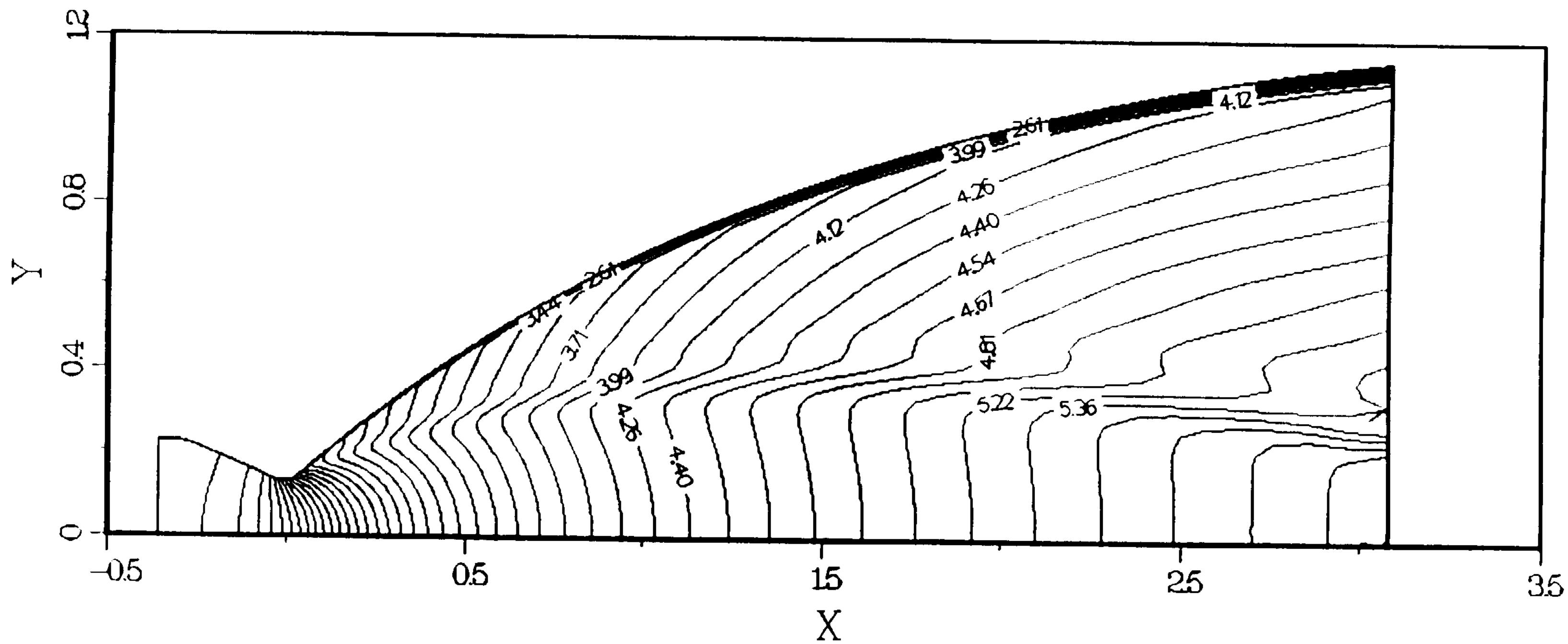

Fig. 9a Contour of Mach number for k-ϵ with two-layer model.

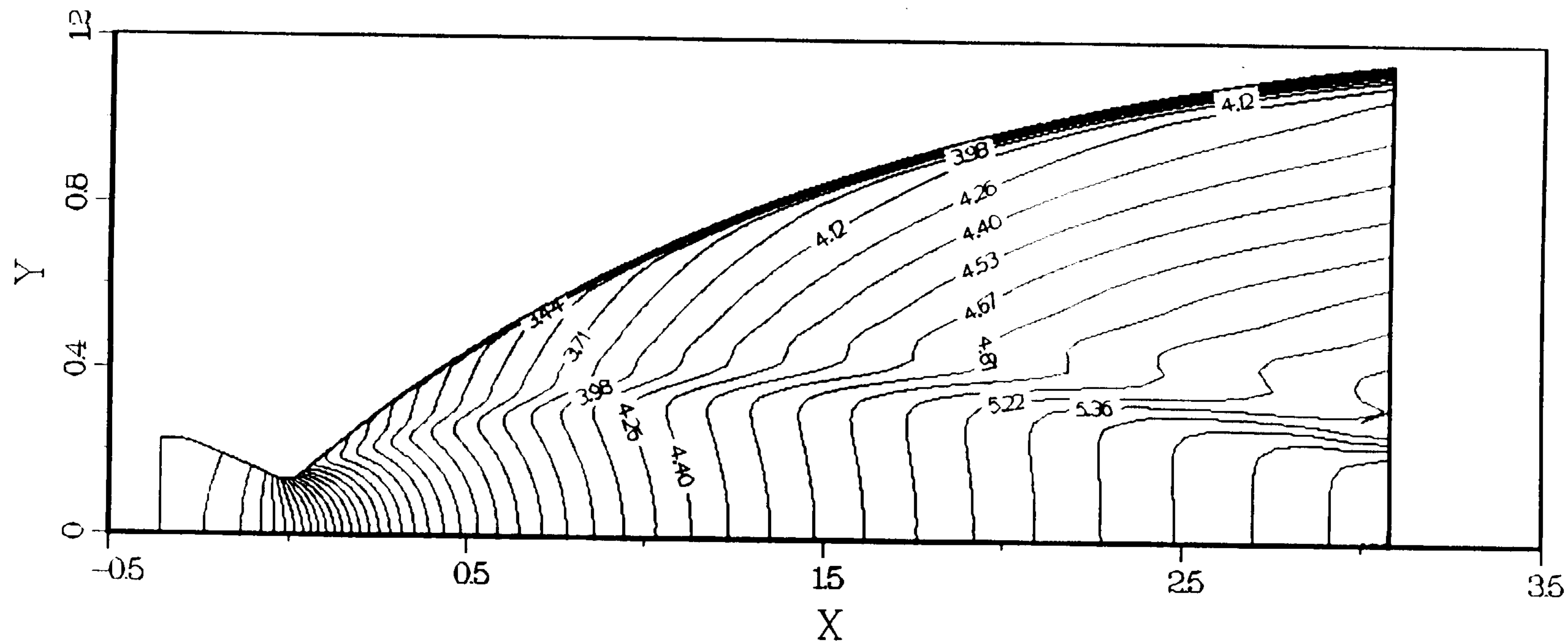

Fig. 9b Contour of Mach number for ASM with two-layer model.

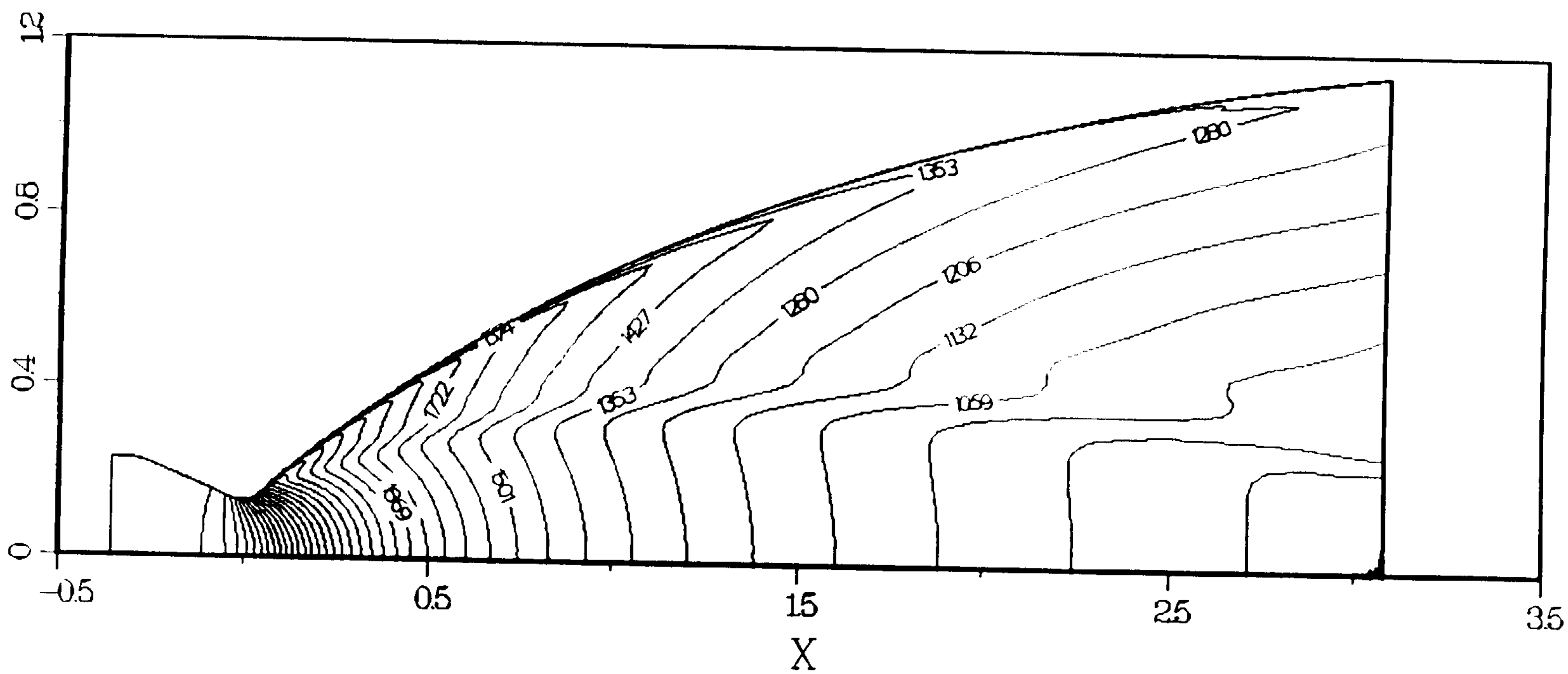

Fig. 10a Contour of temperature for k-ϵ with two-layer model.

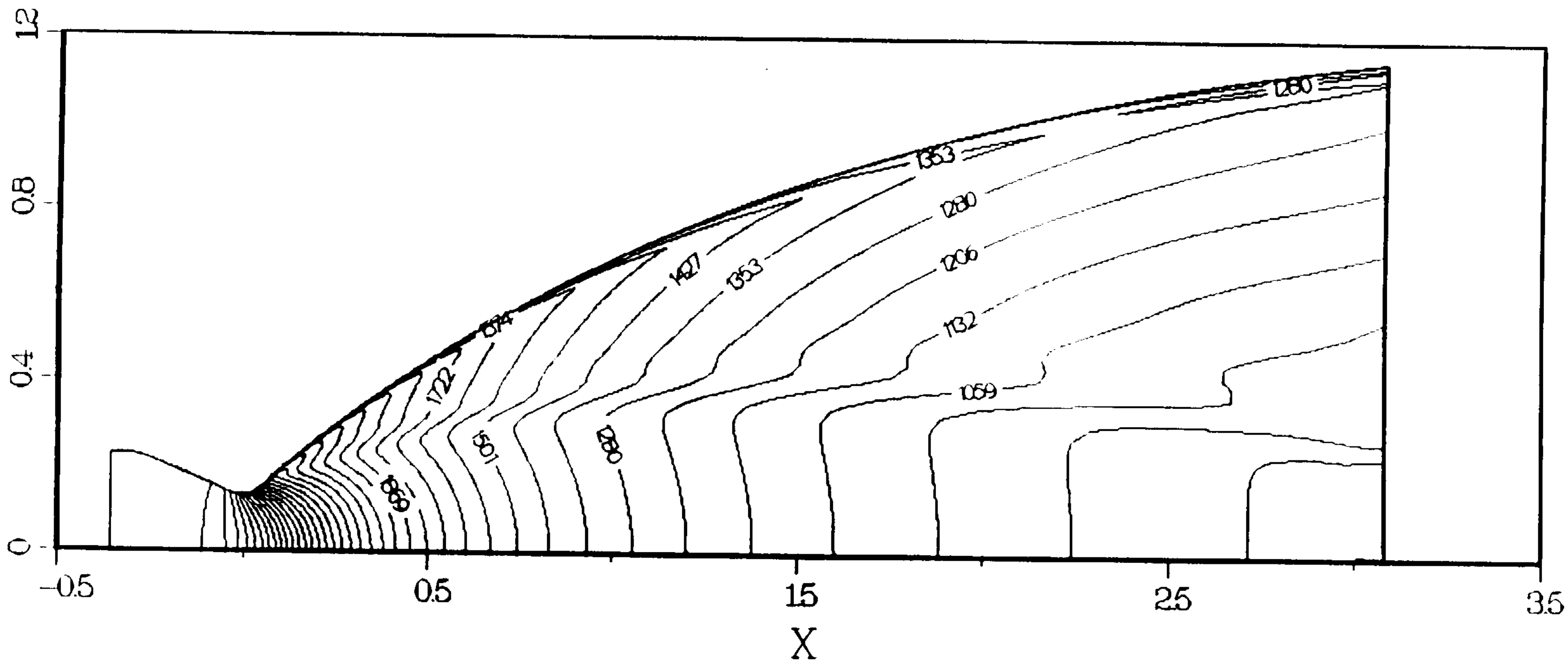

Fig. 10b Contour of temperature for ASM with two-layer model.

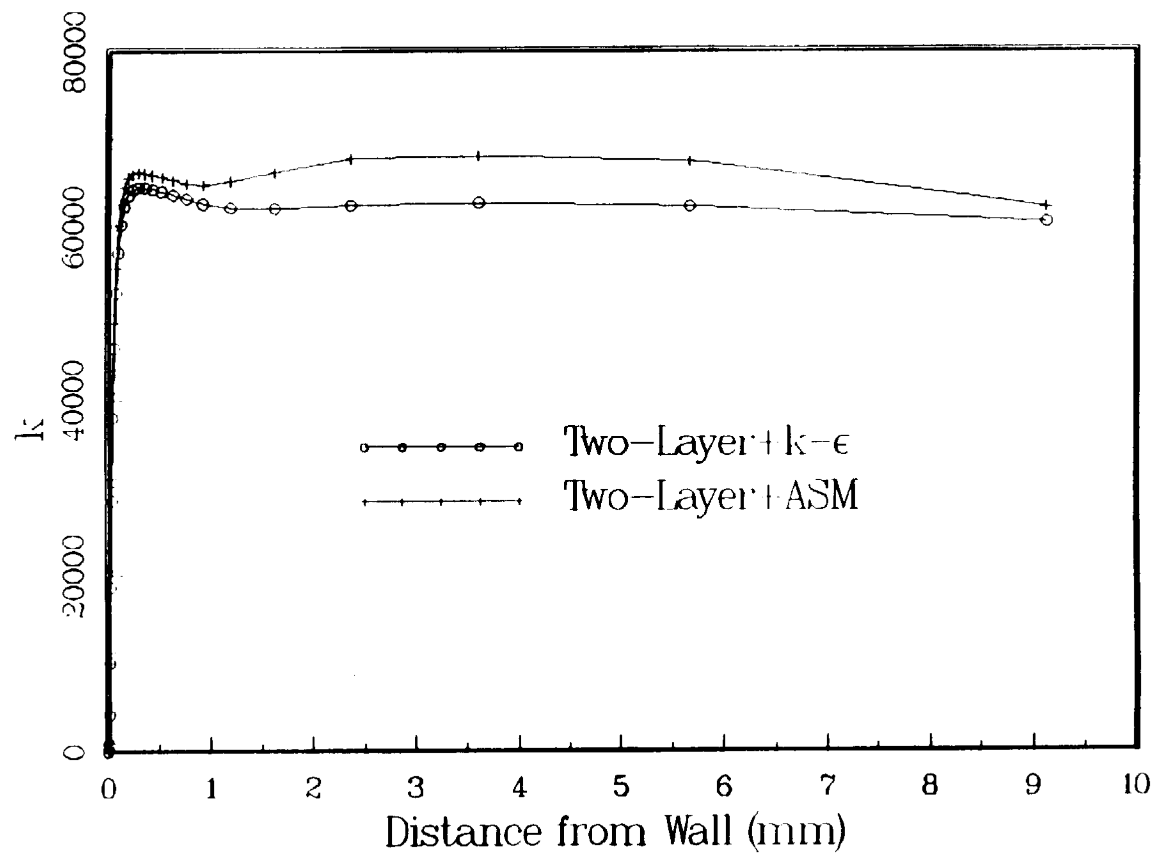

Fig. 11 Behavior of near wall TKE at nozzle exit.

SSME Wall Contour at Exit

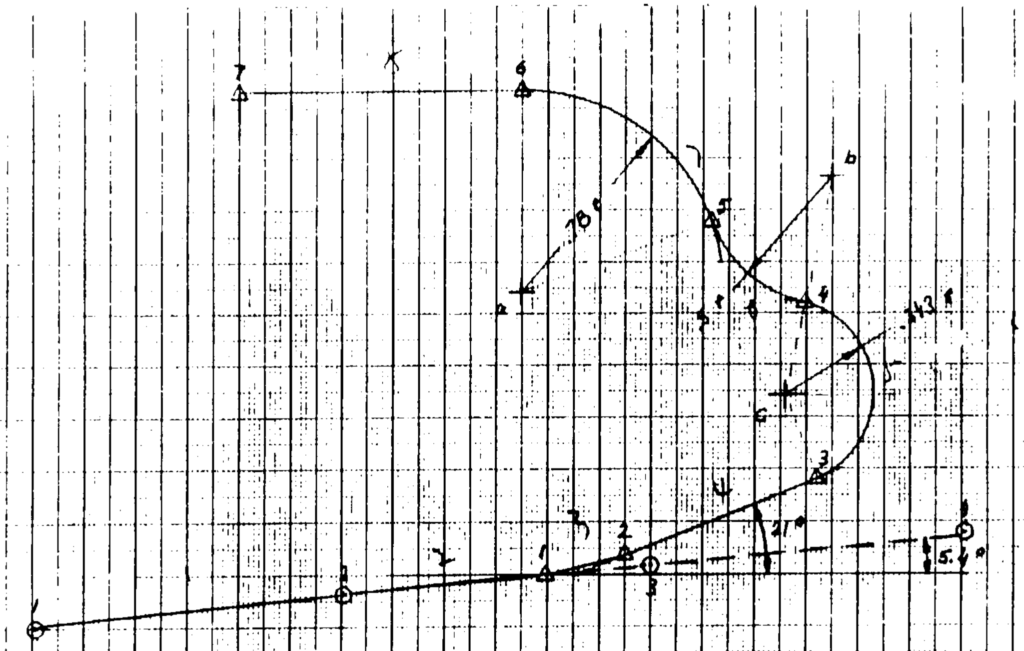

$R_T = 5.1527$ [in]

	x [in]	R [in]	x/R_T	R/R_T
1 ○	8.7348	45.008	22.8246	8.7348
2 ○	8.7583	45.129	23.0574	8.7583
3 ○	8.7812	45.247	23.2905	8.7812
4 ○	8.8034	45.361	22.5232	8.8034
a +	119.478	46.287	23.1875	8.9831
b +	120.7	46.73	23.4246	9.0690
c +	120.518	45.887	23.3893	8.9054

	x [in]	R [in]	x/R_T	R/R_T
1 △	119.578	45.207	23.2069	8.7735
2 △	119.90	45.28	23.2694	8.7816
3 △	120.64	45.36	23.4130	8.8032
4 △	120.60	46.24	23.4052	8.9739
5 △	120.24	46.56	23.3353	9.0360
6 △	119.50	47.07	23.1917	9.1350
7 △	118.40	47.07	22.9782	9.1350

117 118 119 120 121 122 123 X

Fig. 12, SSME wall contour and geometry at exit

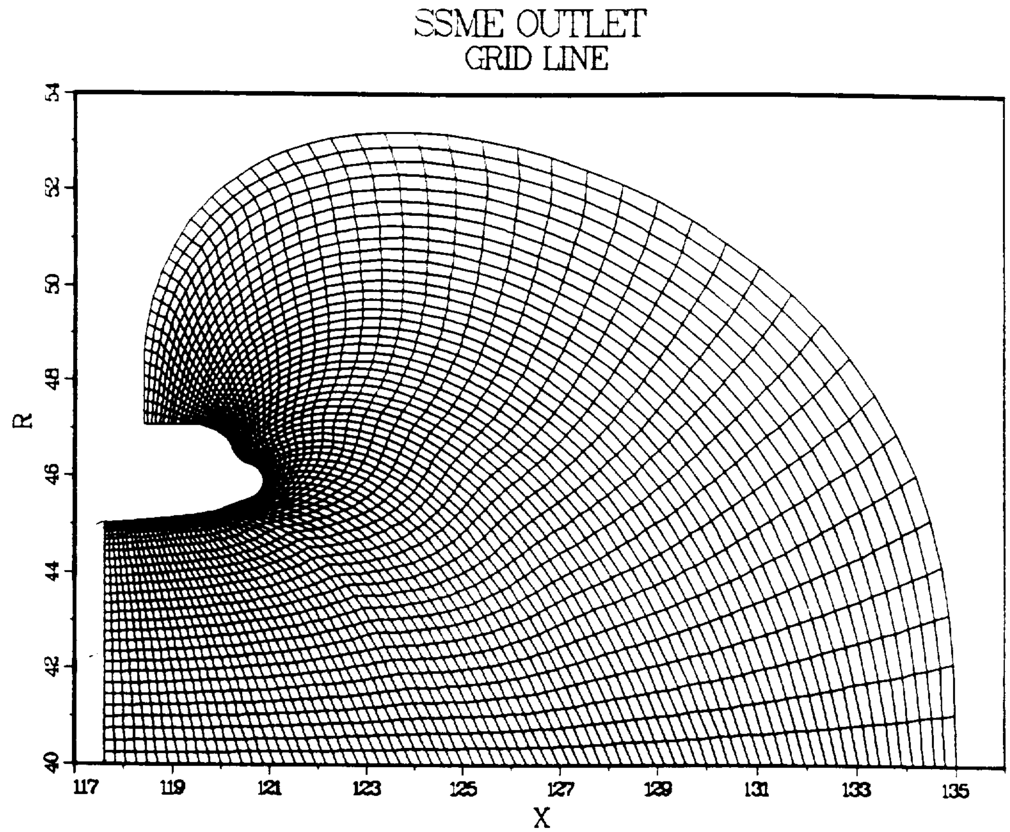

Fig. 13(a), Grid configurations for SSME nozzle exit manifold

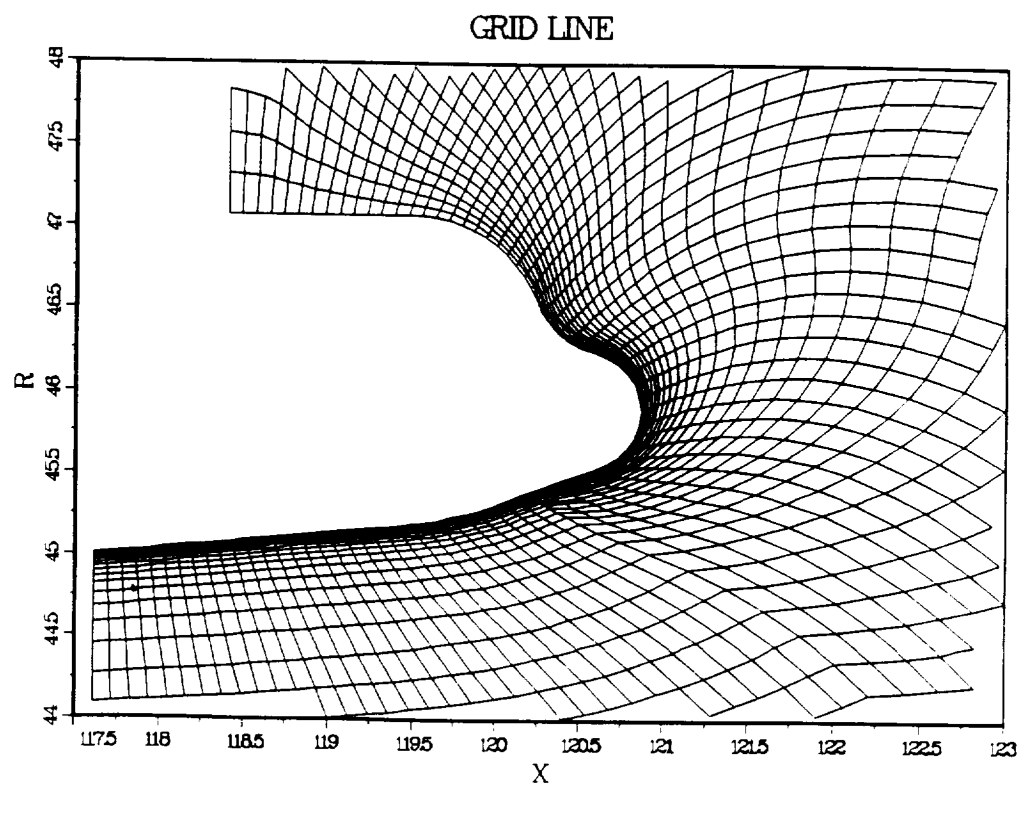

Fig. 13(b), Close-up grids for Figure 13(a)

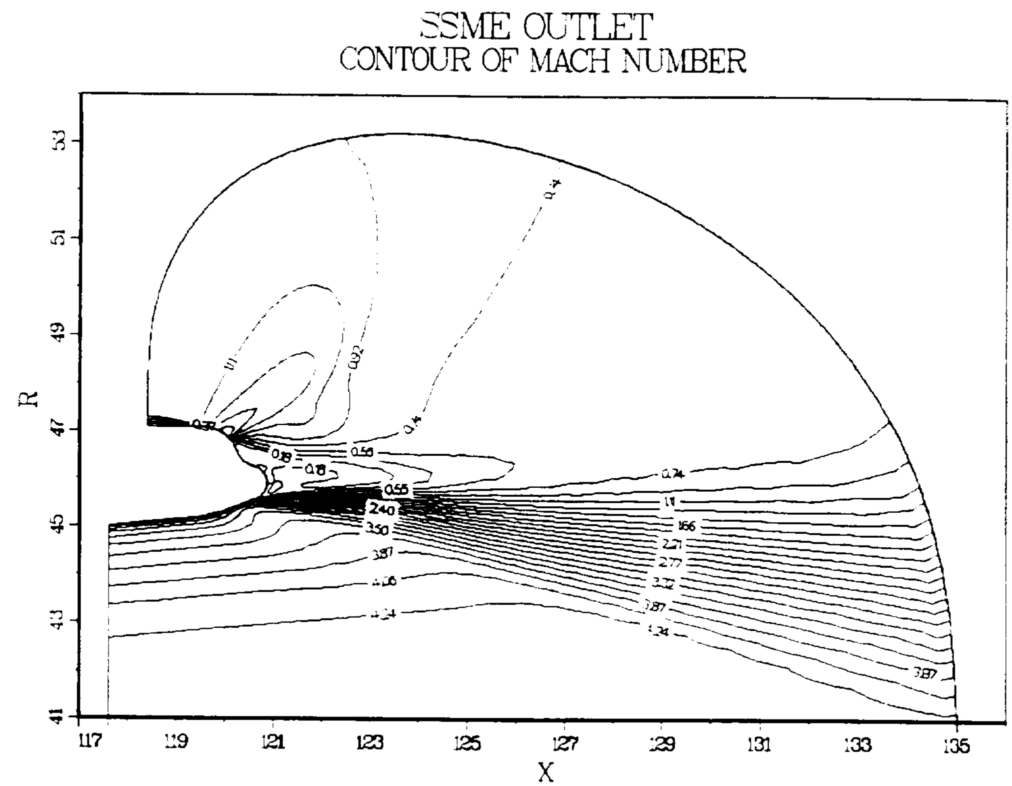

Fig. 14, Contour of Mach number using ASM model

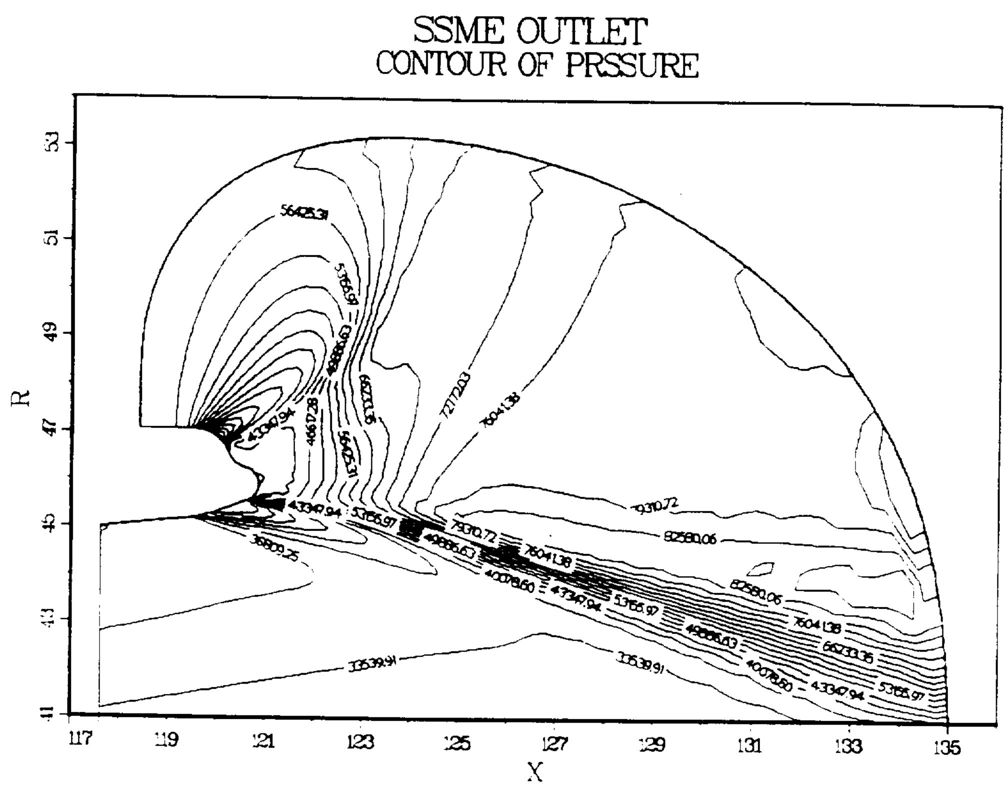

Fig. 15, Contour of pressure using ASM model

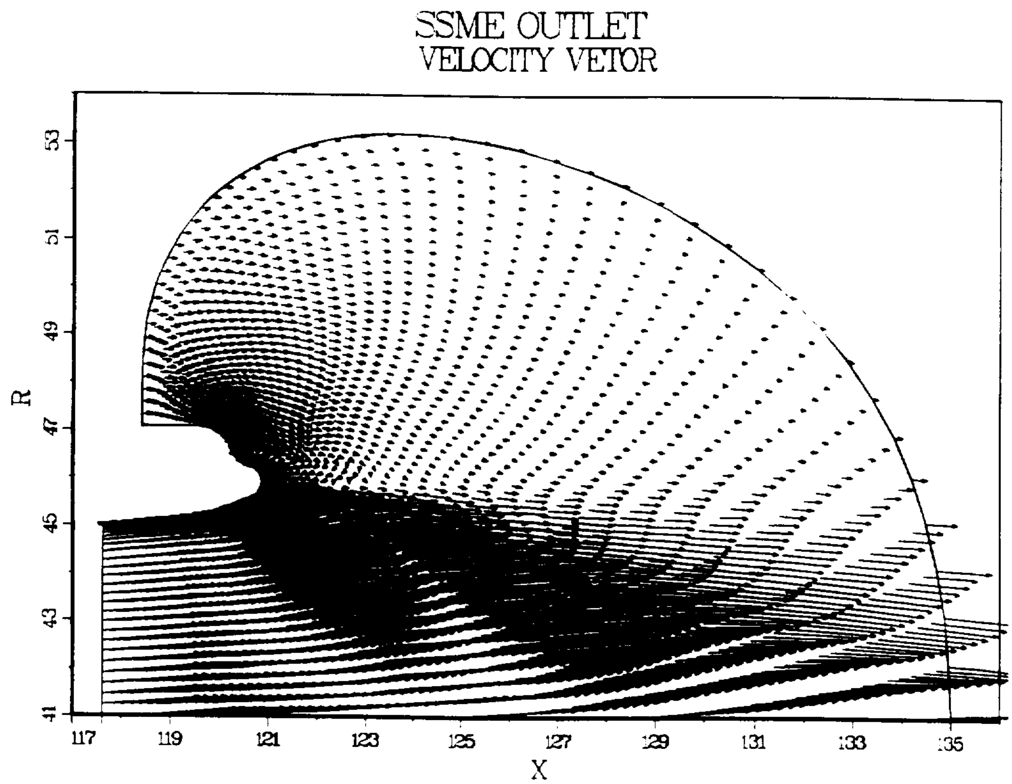

Fig. 16, Vector plot using ASM model

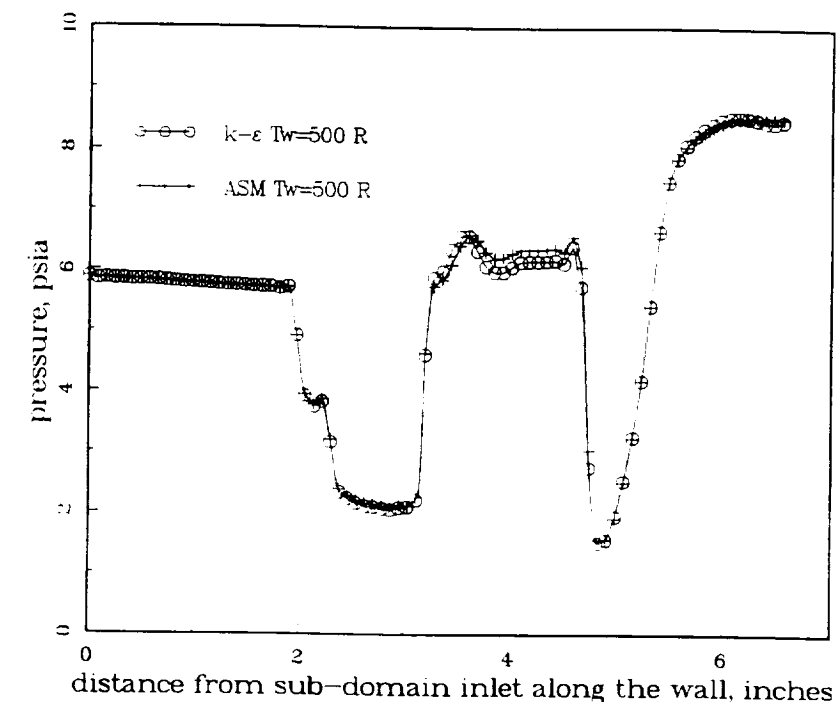

Fig. 17(a), Pressure levels along the wall near the nozzle exit using the ASM and k - ε models

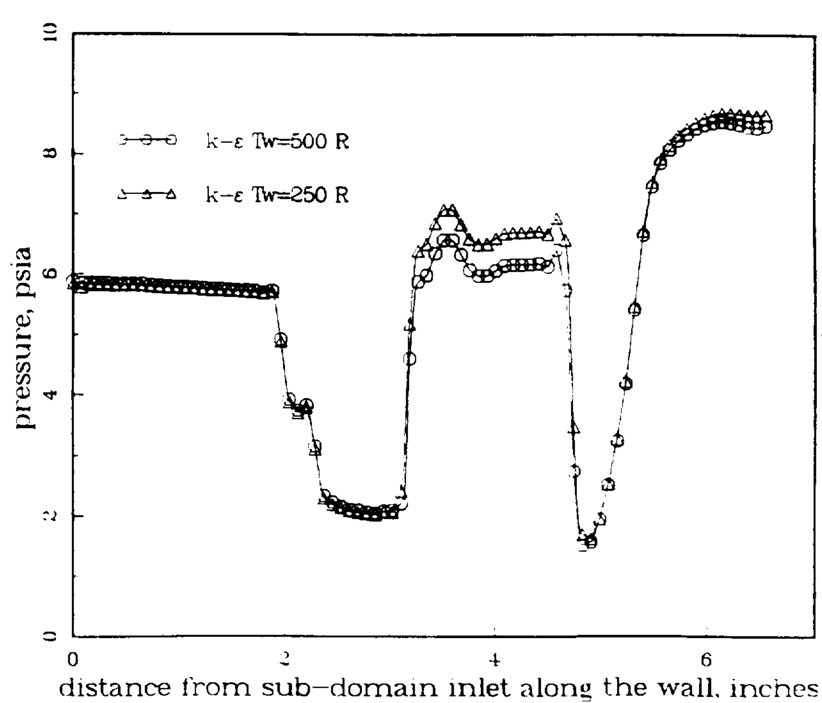

Fig. 17(b), Effects of wall temperature on the wall pressure

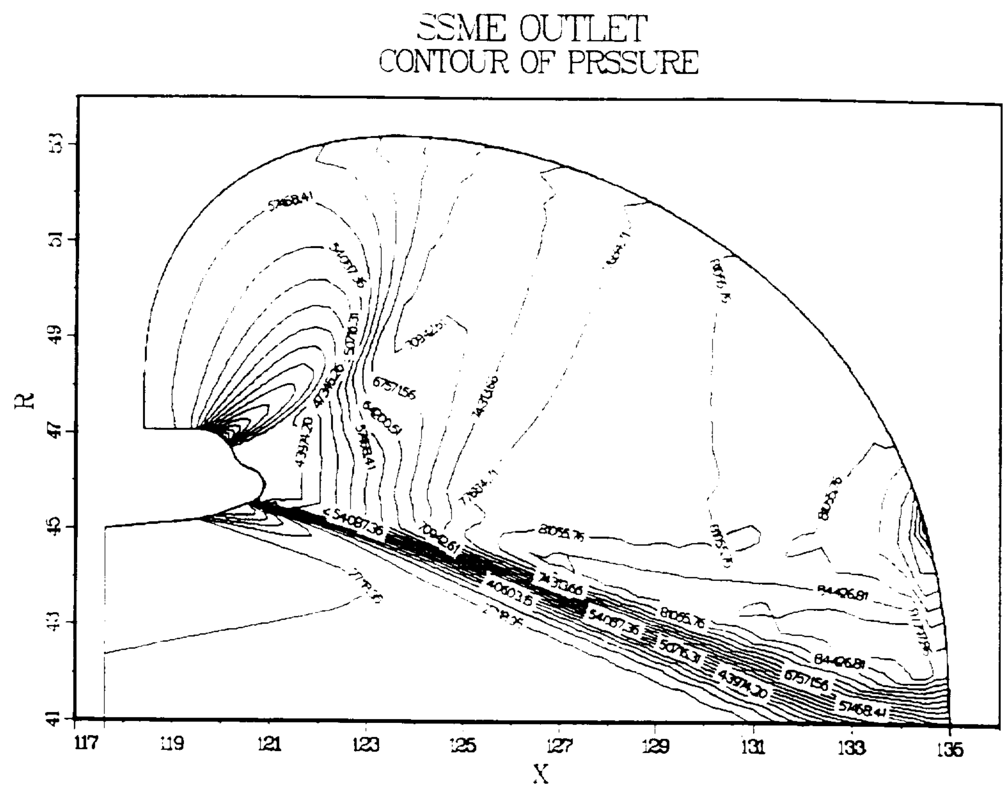

Fig. 18, Contour of pressure using 75% of the chamber pressure level

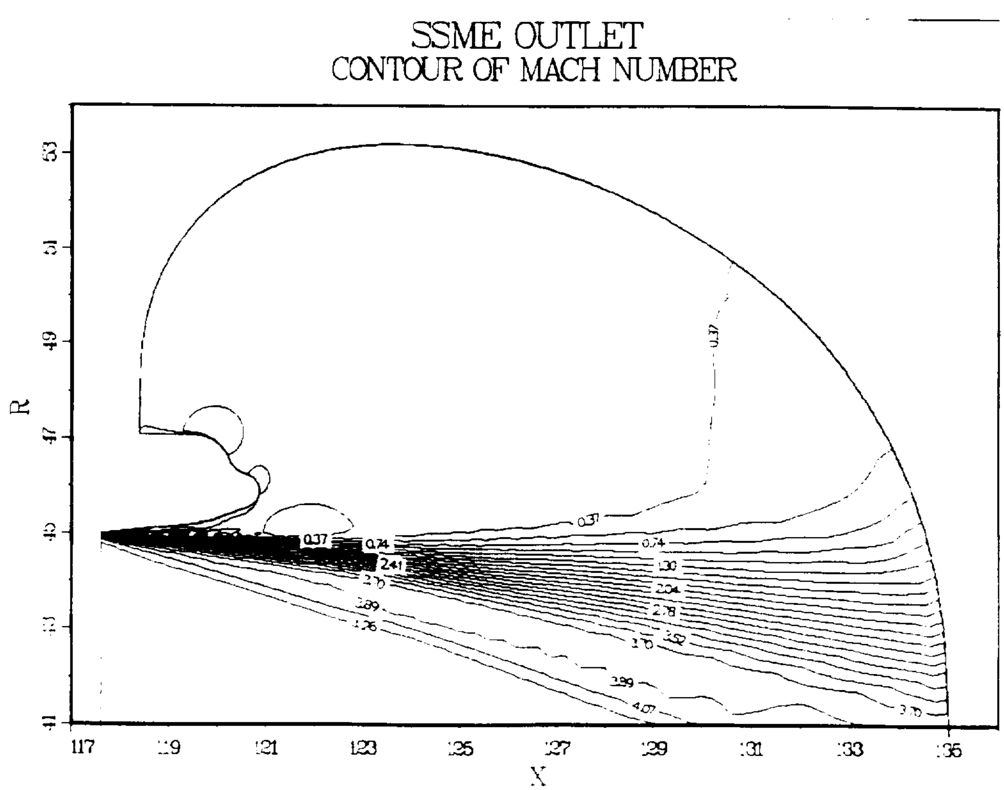

Fig. 19, Laminar flow calculations of the SSME exit flow